Perineuronal nets in cortical processing and plasticity

Master's thesis in Molecular Bioscience
Main field of study in physiology and neurobiology

Kristian Kinden Lensjø

60 study points

Program for Physiology and Neurobiology

Department of Biosciences

The Faculty of Mathematics and Natural Sciences

UNIVERSITY OF OSLO

2013

Acknowledgements

The work presented in this thesis was performed at the Program for Physiology and Neurobiology, Department of Biosciences, University of Oslo, between January 2012 and June 2013, under the supervision of associate professor Dr. Marianne Fyhn, Dr. Torkel Hafting and Dr. Gunnar Dick.

Firstly, I would like to thank my supervisors. Marianne and Torkel for always being positive, for encouraging independence and critical thinking, and of course for all the help with the practical work and writing. Gunnar, for all the help with enzyme work, histology and the writing of this thesis, and for being a realistic voice when the ambition level was set a wee bit too high.

I would like to thank all the members of the Hafting-Fyhn lab. In particular, a big thanks to Dr. Christina Sørensen, Dr. Rachel M. Thomas and Ph.D. student Ida E. J. Aasebø, for helping me with electrophysiology, histology, analysis and writing. For great discussions and sharing frustrations over broken pipettes, misbehaving rats and disappearing cells.

I want to thank all the people at the Program for Physiology and Neurobiology for providing a great educational and social environment.
Family and friends for support, in particular my fellow students Ivan, Olav and Terje.

Oslo, June 2013

Kristian Kinden Lensjø

Abstract

Perineuronal nets (PNNs) are a specialized form of extracellular matrix in the CNS, embodying parvalbumin expressing inhibitory neurons. The PNN assembles towards the end of the period of heightened plasticity, the critical period, in parallel with maturation of the inhibitory network. Degradation of PNNs with the enzyme Chondroitinase ABC (chABC) reopens for plasticity in adults. Together this suggests that PNNs serves as a break on plasticity by stabilizing synapses and maintaining the inhibitory-excitatory balance in the cortex. How the PNN contributes to cortical processing and how its removal opens for plasticity remain elusive.

I investigated how the removal of PNNs in primary visual cortex (V1) influences cortical processing and plasticity in rats, by injecting chABC in V1 and measuring neuronal activity with chronically implanted tetrodes. The PNN was completely degraded after three days, and then reassembled over 60 days. All functional studies were performed within 21 days of enzymatic treatment. Degradation of the PNN caused a non-significant reduction in activity of the inhibitory neurons with more than 50% reduction in mean firing rate compared to controls. Tuning properties, such as orientation selectivity and OD were unaffected.

In order to elucidate how removal of the PNN influences plasticity I used monocular deprivation (MD) to induce activity-dependent plasticity. One eyelid was sutured shut and neuronal activity recorded daily; after five days, the suture was removed and OD reassessed. In accordance with previous studies, MD for five days in the chABC-injected animals produced a shift in OD. Already after one day of MD, neurons contralateral to the deprived eye showed a 50% reduction in firing rate and continued to be reduced throughout the MD period. Conversely, neurons ipsilateral to the deprived eye showed more than 90% increase in firing rate after one day of MD, after which the activity stabilized. The reduced activity of inhibitory neurons after PNN degradation supports the hypothesis that the increased adult plasticity may be caused by a shift in the inhibitory-excitatory balance. The increased activity seen ipsilateral to the deprived eye could be an early indication of a functional change.

I have also studied the effects of anesthesia on cortical processing. For more than 50 years, anesthetized animals have been used to study the visual system. To what extent general anesthetics affect populations of neurons and response properties of single cells have not been determined. I found that neurons in V1 respond very differently to anesthesia; while some were stable or showed increase in firing rate compared to in the awake state, most neurons showed reduced firing rate. Furthermore, the stability in orientation tuning between the two states was highly variable between cells. Altogether, anesthesia should be used with caution when investigating cortical function.

Table of content

1 Introduction

1.1 Plasticity in the central nervous system

Renewal and re-organization are common traits of most mammalian organs; the liver and digestive systems are two examples where renewal and adaptation takes place throughout life. The central nervous system (CNS), however, has been looked upon as rather static, where most of the adaptations and changes occur only early in life. During periods of heightened plasticity in early post-natal development, so called critical periods (CPs), the CNS undergoes large-scale physical and functional changes in order to refine functional neuronal networks, which will produce an adequate response to the external stimuli. Activity-dependent plasticity can be described in terms of functional changes at the synapse, and as changes in structure and connectivity between neurons, where novel synapses are formed or strengthened and others diminish. The CPs have been a target of research for decades and the molecular mechanisms and interplay between different subtypes of neurons during these periods are slowly being unraveled. Changes at the single-synapse level occur throughout life, but the level of plasticity in adulthood is much lower than in young individuals.

1.1.1 Critical period plasticity

Many skills can be learned more easily in childhood than later in life, such as playing an instrument or learning a language. This is a consequence of how our brain develops and, in particular, the occurrence of CPs. Changes in the brain during the CP can be observed at almost every level of magnification; from language learning in humans to single-cell responses and dendritic spine dynamics in visual cortical plasticity in rodents (Wiesel and Hubel, 1963; Johnson and Newport, 1989; Hofer et al., 2009). It has been studied in many areas of the brain, using several model systems, such as visual cortex in cats, primates and rodents, auditory and motor cortex involved in song-learning in birds, somatosensory cortex in primates and auditory cortex in rodents and owls. The timing of the onset and duration of the period varies among species and brain areas (Vaegan and Taylor, 1979; Fagiolini et al., 1994; de Villers-Sidani et al., 2007). Mechanisms underlying control of the onset of the CP are diverse:

while song learning appears to depend to some extent on circadian rhythms (Nordby et al., 2001), the auditory and visual systems depend on sensory stimuli for the period of enhanced plasticity to open (Mower, 1991; Chang and Merzenich, 2003). What they all have in common, however, is that this high susceptibility to learning cannot be matched before the onset or after the closure of the CP. The CPs are essential for correct brain development and the low level of plasticity later in life may serve as protection in the event of time-limited sensory deprivation or brain damage in adulthood. The learned pathways appear to a large extent to be "hard-wired" in the adult. However, if the provided input during the CP is inadequate, this can lead to life-long functional impairments. An example of this is in the case of amblyopia, where input from one of the eyes to the visual cortex during development is impeded, for instance as the result of untreated strabismus. The brain stops "listening" to the weak eye, which leads to blindness, although the eye itself remains functional (Wiesel and Hubel, 1963; Vaegan and Taylor, 1979). The amblyopic model is indeed the most used system to study CP plasticity, due to the fact that the anatomical basis of the visual system is fairly well understood, the sensory inputs are easily controlled and manipulated, and the anatomical localization of the visual cortex is favorably located for recording neuronal activity.

1.1.2 The visual system and ocular dominance

When photoreceptors in the retina of mammals are activated, the signal is transferred through ganglion cells to the dorsal part of the lateral geniculate nucleus (dLGN) of the thalamus. Cells from the dLGN synapse onto layer IV neurons in the primary visual cortex (V1), and the signal is further transferred to extrastriate areas (figure 1.1). The ganglion cells receive input from a large number of photoreceptors, usually located within a tiny patch of the retina; one such patch makes up a ganglion cell's receptive field. Ganglion cells can be classified as "on-center" and "off-center" cells: on-center cells fire bursts of action potentials when their receptive field is illuminated, while off-center cells are inhibited by illumination of their receptive field, followed by bursts of action potentials as the illumination ends (Kuffler, 1953). These receptive fields are overlapping, and cover the entire retinal surface. Many on- and off-center

cells converge onto the same dLGN cell and many such dLGN cells further converge onto the same cell in V1. The retinotopic organization is maintained through the dLGN to the V1. This organization means that, both in the dLGN and in V1, the cells' receptive fields will be shaped by excitatory and inhibitory input. The high degree of convergence in the visual system allows cells in the cortex to be "tuned" to specific stimuli: so-called simple cells detect edges of a specific angle, while others, the so-called complex cells, detect edges with a specific direction of motion (Hubel and Wiesel, 1959). Despite parallel paths in the ganglion cells and through the dLGN, V1 is the first site where input from both eyes converges and compete at the synaptic level.

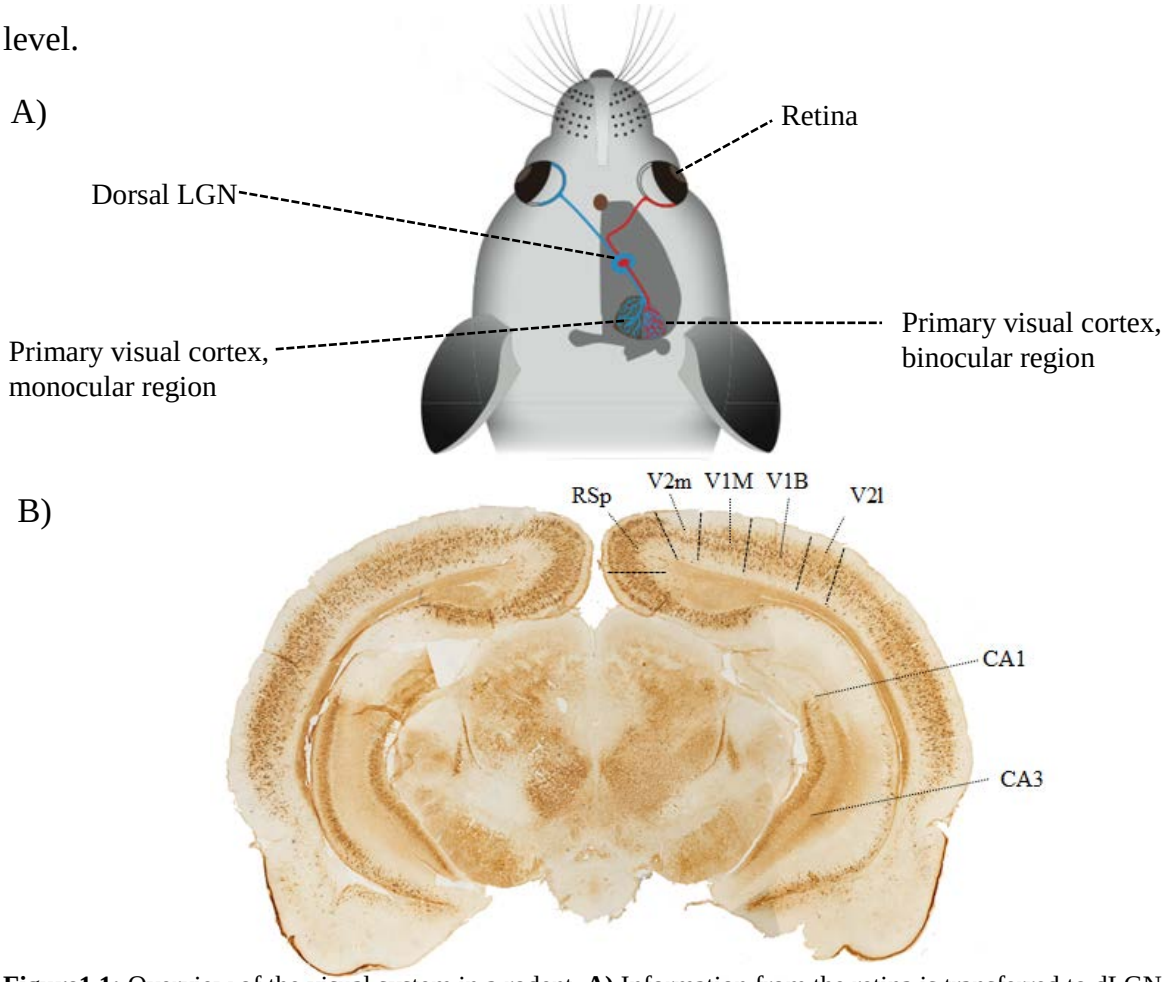

Figure1.1: Overview of the visual system in a rodent. **A)** Information from the retina is transferred to dLGN, and further to the primary visual cortex (V1). The binocular region of V1 is the first site where input from both eyes competes. (Adapted from Leeveld & Hübener, 2012) **B)** A coronal section from a rat brain, showing the functional organization in the cortex. The section is stained with Wisteria floribunda agglutinin (WFA), labeling perineuronal nets. Rsp = Retrosplenial cortex, V2m = Medial secondary visual cortex, V1M = Primary visual cortex, monocular region, V1B = primary visual cortex, binocular region, V2l = Lateral secondary visual cortex, CA1 = CA1 region of the hippocampus, CA3 = CA3 region of the hippocampus. Lensjø, Dick, Hafting & Fyhn (unpublished).

The outcome of the competition in V1 is determined during the CP. For excitatory pyramidal cells, the result is that a majority will respond stronger (i.e., have a higher rate of action potentials) to stimulation of one of the eyes, as opposed to stimulation of the other (Hubel and Wiesel, 1962). This property is called ocular dominance (OD). In higher mammals, such as primates and carnivores, cells that share the same OD preference tend to be organized together in columns across V1 (Mountcastle et al., 1955; Hubel et al., 1976; Shatz and Stryker, 1978; Horton, J. C. and Hocking, D. R., 1996). The idea that the columnar organization is the result of CP competition alone, however, may not be true; findings indicate that thalamocortical afferents (i.e., neurons from the dLGN to V1) are clustered together in a similar pattern before the CP begins (Des Rosiers et al., 1978; Horton, J. and Hocking, D., 1996). The columnar organization may be established earlier in development by molecular cues.

The phenomenon of OD has been the basis for using the visual cortex as a model in CP plasticity research, as closure of one of the eyes during the CP induces a shift in OD. This was first described by David Hubel and Torsten Wiesel, when they showed that closure of one eye of kittens caused a dramatic shift in cortical activation and OD distribution towards the non-deprived eye (Wiesel and Hubel, 1963). In rodents, OD is present in individual neurons in the binocular region of V1, which receives input from both eyes. These cells are not organized in OD columns, but instead appear to be randomly distributed (Drager, 1978). In juvenile mice, closing one of the eyes for only a few days during the CP is enough to produce a marked shift in OD (Drager, 1978; Gordon and Stryker, 1996). The changes that happen during such a short period of sensory deprivation occurs mainly at the synaptic level, while sensory deprivation over time has a profound structural impact in the thalamocortical pathway and may eventually cause blindness (Headon and Powell, 1973; Antonini and Stryker, 1996).

1.1.3 Onset of the critical period – development of the inhibitory system

Two major events are implicated in the onset of the CP for vision, namely sensory stimulation after eye-opening and subsequent development and maturation of the inhibitory network. Animals reared in the dark from birth show postponed CP, indicating that sensory input to V1 is necessary to initiate the CP (Mower, 1991;

Fagiolini et al., 1994). With normal visual stimulation after eye-opening, pyramidal cells start to synthesize and secrete the growth factor brain-derived neurotrophic factor (BDNF) (Zafra et al., 1990). Subsequently, BDNF triggers growth and maturation of inhibitory neurons (Hanover et al., 1999; Huang et al., 1999). The most abundant inhibitory neurotransmitter in the brain is gamma-amino butyric acid (GABA). Infusion with the GABA agonist benzodiazepine in the visual cortex prior to the normal onset age of the CP, as well as transgenic overexpression of BDNF, will accelerate the onset of the CP (Huang et al., 1999; Fagiolini and Hensch, 2000; Iwai et al., 2003). Furthermore, mouse models with reduced GABA synthesis, due to a deletion of the gene coding for the enzyme glutamic acid carboxylase GAD65, do not undergo a CP unless it is artificially induced by treatment with the GABA agonist benzodiazepine (Hensch et al., 1998). Based on this finding, it has been suggested that during development of the inhibitory neuronal network the cortical circuitry reaches a specific window in the inhibitory-excitatory balance that allows for the elevated plasticity, while in adults the level of inhibition, and thus the inhibitory-excitatory balance, is above this threshold (Fagiolini and Hensch, 2000). The pivotal role of inhibition in CP plasticity is well established; however, how or even if it contributes at all to plasticity in the adult remains largely unknown.

1.1.4 Parvalbumin expressing inhibitory neurons

Inhibitory interneurons have been categorized based on morphology, function and protein expression, and not all GABAergic neurons are involved in plasticity (Fagiolini et al., 2004). The GABAergic neurons that express the calcium binding protein parvalbumin (PV^+) seem to play a particularly important role in the regulation of plasticity. Many of these neurons correspond to a class of inhibitory neurons called basket cells (Klausberger et al., 2002). They are characterized by bursts of high frequency action potentials and form a large network, synapsing onto the soma of pyramidal cells as well as each other (Kawaguchi and Kubota, 1997; Buzás et al., 2001; Galarreta and Hestrin, 2002). The PV^+ inhibitory cells integrate and mature into the visual cortex at the onset of the CP (Del Rio et al., 1994), where they seem ideally positioned to regulate and stimulate synchrony throughout a population of neurons

(Tamás et al., 1997; Meyer et al., 2002). One of the exceptional features of the PV^+ cells is their ability to fire bursts of action potentials with very high frequency (Erisir et al., 1999). This is largely due to the high abundance of a subclass of voltage gated potassium channels, the Kv3 ion channels (Rudy and McBain, 2001), in particular Kv3.1 subunits, specifically expressed in PV^+ cells (Weiser et al., 1995; Sekirnjak et al., 1997). In addition to the Kv3 channels, the cells they synapse onto almost exclusively utilize alfa-1 subunits in their GABA receptors, the subunit class with the fastest decay times (Nusser et al., 1996; Klausberger et al., 2002). In mouse models where the alfa-1 subunit has been rendered insensitive to benzodiazepines, the CP cannot be induced early by benzodiazepine treatment (Fagiolini et al., 2004), suggesting that the fast transmission is an essential feature of the inhibitory system for regulating plasticity.

In addition to BDNF, the protein Orthodenticle homeobox 2 (Otx2) is vital for the maturation of inhibitory neurons. It is synthesized in the retina upon visual stimulation and transported through the dLGN and further to V1 where it is taken up predominately by PV^+ cells (Sugiyama et al., 2008) and stimulates their maturation. Otx2 removal from the visual pathway completely abolishes plasticity. Interestingly, maturation of the PV^+ cells does not depend on direct neuronal input from the dLGN, but instead indirect input through activity in neighboring cortical excitatory cells (Chattopadhyaya et al., 2004; Cristo et al., 2004; Patz et al., 2004). The combined actions of Otx2 from the retina and BDNF from neighboring cells appear to be the triggers for the PV^+ cells to mature.

In addition to their role in plasticity, PV^+ inhibitory neurons have been shown to be an important regulator and synchronizer of the slower brain oscillations, for local populations of neurons. These oscillations are the combined output of the activity of all the cells within an area and correlates with physical activity and cognitive function (Freund, 2003). They can be recorded by the use of an electroencephalogram (EEG). Oscillations in the gamma frequency band, i.e. 30-80 Hz, have been implicated in the process of information transfer between brain areas, and oscillations within this band are initiated locally by the PV^+ cells (Ylinen et al., 1995; Freund, 2003).

1.1.5 Adult plasticity

The level of plasticity during the CP cannot be matched later in life (Wiesel and Hubel, 1963; Hubel et al., 1976; Drager, 1978; Sato and Stryker, 2008). However, synaptic modification in the form of long-term potentiation (LTP) and long-term depression (LTD) is possible to some extent even in adulthood (Bliss and Lomo, 1973; Levy and Steward, 1979; Racine et al., 1995). In the hippocampus, a part of the brain heavily associated with learning and memory formation, adult-born neurons remain susceptible to change, and the hippocampal structure keeps a high level of plasticity (Levy and Steward, 1979; Lemaire et al., 2012). LTP and LTD are also seen in the neocortex, but to a somewhat lesser extent; induction here requires stronger stimuli and is mainly seen in relation to motor learning and long term sensory deprivation in connection to injury (Jenkins and Merzenich, 1987; Iriki et al., 1989; Trepel and Racine, 1998). Upon extended periods of sensory deprivation, some functional changes have been observed including receptive field size changes in the somatosensory, auditory and visual cortices, and rearing animals in environments with complex stimuli increases dendritic spine dynamics, a feature related to synaptic reorganization (Rosenzweig et al., 1964; Greenough et al., 1973; Merzenich et al., 1984; Eysel and Schweigart, 1999; Blake and Merzenich, 2002). In addition, if a sensory area is damaged, an adjacent area can adopt some of the function; for instance, damage to the cortical sensory areas related to the vestibular system can be rescued by other nearby sensory areas, provided the sensory input is adapted to something the new area can translate (i.e., somatosensory stimulus) (Bach-y-Rita and W. Kercel, 2003).

Nonetheless, the ability of the CNS for repair and regeneration is relatively poor. Reopening for plasticity in adults could prove to be an immense aid for the recovery from both CNS damage, in the form of physical damage and stroke, and developmental disorders. One of the key players involved in restricting plasticity in adulthood seems to be the proteoglycans in the extracellular matrix.

1.2 Extracellular matrix in the CNS

The extracellular matrix (ECM) composition in the CNS differs from the rest of the body. Proteoglycans, hyaluronic acid, link proteins and tenascins are the main components, while fibrous proteins such collagen, fibronectin and elastin are nonexistent in the CNS. Among the proteoglycans, the lectican-family members versican (isoform 2), aggrecan, brevican, phosphacan and neurocan are expressed in the CNS (Rauch et al., 1991; Asher et al., 1995; Yamada et al., 1997; Schmalfeldt et al., 1998). These are all modified by chondroitin sulfate (CS). The ECM in the CNS is involved in brain development through axonal guidance and injury repair and seems to be directly involved in regulating plasticity (Kwok et al., 2011; Myers et al., 2011; Wang and Fawcett, 2012).

1.2.1 Proteoglycans in the CNS

Proteoglycans (PGs), together with hyaluronic acid, make up a vast majority of the macromolecular part of the extracellular space in the CNS (Margolis et al., 1975; Yamaguchi, 2000). PGs are glycoproteins extensively modified by a specific type of glycosylation; glycosaminoglycan (GAG) chains. PGs carry one or several GAG chains, in addition to N- and O-linked oligosaccharides. The GAG chains are unbranched polymers made up of sulfated disaccharides, covalently bound to the protein core, usually through an O-linkage to a serine residue. Each disaccharide consists of an uronic acid and an amino sugar, e.g., N-acetylgalactosamin or N-acetylglucosamin. The identity of these sugars is the basis for the categorization of GAGs into keratan sulfates (KS), heparin/heparan sulfates (HS) and dermatan/chondroitin sulfates (DS/CS) (Prydz and Dalen, 2000). The chains vary in length from 2-200 disaccharides, and PGs can carry hundreds of them. Hyaluronic acid has a structure similar to the GAGs of PGs: it is essentially a single, large GAG polymer, not bound to a protein core, and not modified by sulfation. The negative charges carried by the carboxyl and sulfate groups give the GAGs, and hence also the PGs, a strong negative charge.

PGs are categorized on the basis of their GAG chains into keratan sulfate PGs (KSPGs), heparin sulfate PGs (HSPGs) and chondroitin sulfate PGs (CSPGs). The CSPGs have been of particular interest, not only due to their prominence in the CNS, but also due to the role this subclass seems to play in connection to injury repair and plasticity in the CNS. Upon injury to the CNS, astrocytes, microglia and pericytes start to proliferate and migrate toward the injured site and form what is known as the glial scar (Hatten et al., 1991; McKeon et al., 1991; Goritz et al., 2011). The glial scar is believed to have a protective effect, in that it prevents the spread of toxic release from the damaged cells (Pindzola et al., 1993; McKeon et al., 1995; Bush et al., 1999). Synthesis and secretion of PGs, especially CSPGs, is up-regulated in the glial scar, for reasons that are not yet fully understood (McKeon et al., 1991). CSPGs have an inhibitory effect on neuronal regeneration and axonal outgrowth (Snow et al., 1994; Coles et al., 2011).

1.2.2 The perineuronal net

The perineuronal net (PNN) is a highly condensed form of ECM found in sub-populations of neurons in the CNS, which was discovered late in the 19th century (Golgi, 1898). It has been identified in the spinal cord and several areas of the brain (Hockfield and McKay, 1983; Brauer et al., 1993). The PNN wraps tightly around the soma and proximal dendrites of neurons in a lattice-like formation (figure 1.2), consisting of several of the same components that are used in cartilage (e.g., hyaluronic acid, link proteins, CSPGs and the CNS-associated tenascin-R) (Carulli et al., 2006; Deepa et al., 2006). The tight organization arises through interactions between CSPGs and cell membrane-bound, unsulfated hyaluronic acid. These interactions are stabilized by link proteins and further supported by interactions between tenascin-R and the core protein of CSPGs (Lundell et al., 2004). The compact organization only opens up around synapses and could in part explain the low level of synaptogenesis seen in adults.

A)

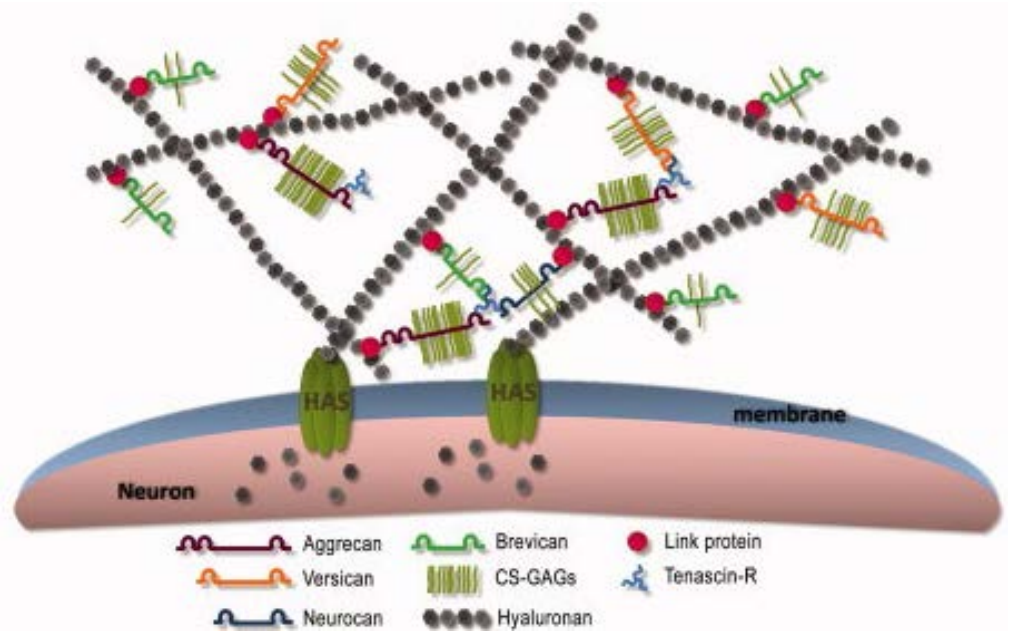

B)

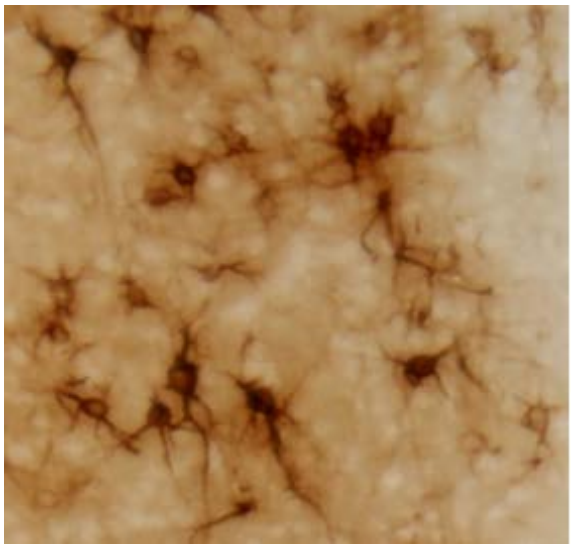

Figure 1.2: Proposed structure of the perineuronal net (PNN). **A)** HAS are hyaluronic acid synthetases, located on the cell membrane. They synthesize hyaluronic acid, which is secreted in the extracellular space, where they form the backbone of the PNN. Adapted from Kwok *et al.* (2011). **B)** PNNs, labeled with the lectin *Wisteria floribunda* agglutinin (WFA), wrapped around the cell body and dendrites of neurons in primary visual cortex. Lensjø, Dick, Hafting & Fyhn (unpublished).

1.2.3 The perineuronal net and plasticity

The formation of the PNN coincides with the end of the critical period (Hockfield et al., 1990). The assembly is activity-dependent and a lack of stimuli (e.g., through dark rearing of animals) can prolong the CP and postpone the formation of the PNN (Pizzorusso et al., 2006; Dityatev et al., 2007; McRae et al., 2007; Ye and Miao, 2013). The PNN can be degraded by the use of a bacterial enzyme, Chondroitinase ABC (chABC), which cleaves the CS GAG chains into disaccharides (Brückner et al., 1998). Treatment with chABC has been shown to lead to CP-like levels of plasticity,

where a shift in OD can be induced in a matter of days in adult rats (Pizzorusso et al., 2002; Pizzorusso et al., 2006). Animal models where the link protein of the PNN is genetically deleted, also show increased OD plasticity (Carulli et al., 2010). Together, these results support the idea that the formation of the PNN is involved in the closure of the CP. Treatment with chABC has also been shown to increase plasticity in other systems such as fear-conditioning, indicating that the increase in plasticity following chABC treatment is a general concept (Gogolla et al., 2009). After chABC injection, the PNNs are gradually reassembled over a time-span of 30-150 days (Brückner et al., 1998). A more temporally accurate description of the reassembly of the PNN has not been reported.

Most of the attention with respect to chABC treatment, however, has been in relation to the glial scar. Enzymatic digestion of the CSPGs in the glial scar has been shown to improve the anatomical and functional outcome in animal models of spinal cord injury and stroke (Bradbury et al., 2002; Hill et al., 2012; Soleman et al., 2012). Treatment with chABC promotes axon growth both in injured and intact fibers in the spinal cord, and is currently in development as a therapeutic agent to aid rehabilitation in patients with spinal cord injury (Barritt et al., 2006; Massey et al., 2006). As CSPGs are the main components of the glial scar as well as the PNN, the mechanisms reported in relation to spinal-cord injury are highly relevant to chABC digestion of the PNN. Indeed, some of the observed effects of chABC treatment after injury could also be a result of digestion of the PNN in the spinal cord.

Interestingly, the PNNs are mainly condensed around PV^+ interneurons (figure 1.3) (Brauer et al., 1993; Hartig et al., 1994; Härtig et al., 1999; Morris and Henderson, 2000). The highly negative charge of the GAGs in the PNN could help facilitate the fast-spiking activity in the PV+ cells by providing a suitable ionic milieu that binds sodium, calcium and potassium, working almost like a cation exchanger. Indeed, ion balance in the form of extracellular calcium diffusion and intracellular calcium concentrations are disturbed when the PNN is disrupted by chABC treatment (Snow et al., 1994; Hrabetova et al., 2009). Another possible interplay between PV^+ cells and the PNN is the capture and transfer of Otx2: the CS GAGs recognize and bind a

specific amino acid sequence in Otx2 (Beurdeley et al., 2012). Prior to the assembly of the PNN, CSPGs are found in the ECM, however, the assembly and specific localization around PV^+ cells does not happen until the CP comes to an end. Thus, the PNN seems to be involved in several mechanisms regulating plasticity in the adult CNS, although its role in normal processing is largely unknown.

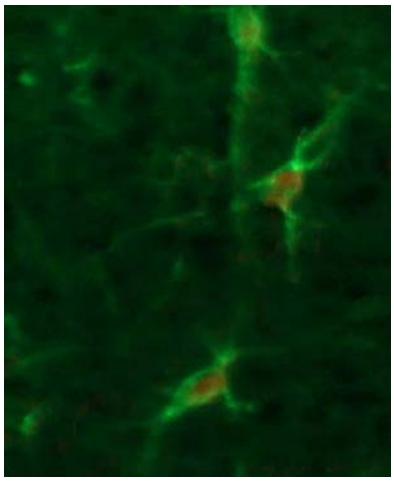

Figure 1.3: Perineuronal nets (green) mainly assemble around parvalbumin expressing inhibitory neurons (red) towards the end of the CP. The extent of the co-localization has not been quantified in V1. The section is stained with WFA and rabbit anti-parvalbumin. Lensjø, Dick, Hafting & Fyhn (unpublished).

1.2.4 Proteinases in development and plasticity

Modifications to ECM in the form of proteolytic cleavage occur continuously, both during development and in adulthood. Of particular interest has been the matrix metalloproteinase (MMP) family; these proteases have previously been implicated in several diseases, though recent findings indicate that they play a large role in development of the CNS and adult plasticity (Ethell and Ethell, 2007; Van Hove et al., 2012). MMPs seem to be important for LTP, dendritic spine remodeling, synapse remodeling, and, to some extent, CP plasticity (Bozdagi et al., 2007; Gundelfinger et al., 2010; Spolidoro et al., 2011). Although there are many molecular targets for MMPs, under normal conditions the digestion seems to cause more profound functional rather than structural changes. In addition to MMPs, the protease tissue plasminogen activator (tPA) is essential for development in the CNS; in fact, if tPA activity is blocked, the CP is not initiated (Mataga et al., 2002). While MMPs and tPA show effects influencing CP plasticity and may even affect PNN structure by protein degradation, chABC acts on the vital components of the PNN and disrupt their structure by potent degradation of GAGs.

1.3 Effects of anesthesia

Ever since Hubel and Wiesel discovered visual responses in the late 1950's, anesthetized animals have been preferred for the study of the visual system. When assessing specific tuning properties of single cells such as orientation selectivity, it is obviously advantageous that the animal lie still or the ever changing angle of the head would disturb the experiment. Head-restraining animals could provide a solution to this problem, but anesthesia is by far what has been used the most. However, general anesthetics have severe effects on the CNS and could thus potentially give rise to skewed data. The GABAergic system is a known target for many general anesthetics and modulation of this system could affect the specific properties of target cells to inhibition in the sensory cortices (Franks, 2008). Recent reports indicate that during anesthesia tuning properties remain the same, though the average firing rates of neuronal populations are significantly reduced, burst firing is abolished, astrocyte signaling is heavily affected and receptive field properties of single neurons may change (Greenberg et al., 2008; Niell and Stryker, 2010; Thrane et al., 2012). Altogether, the use of anesthesia has severe effects on normal processing in the brain.

1.4 Aims of the study

The main objective of this study was to elucidate how PNNs contribute to normal processing and plasticity in the visual cortex, and how anesthesia affects single cells and populations of neurons in the visual system. This was achieved by addressing the following:

- determining how long it takes for PNNs to reassemble after enzymatic degradation

- investigating the effects of degradation of the PNN on cortical processing in the visual system

- investigating the effects over time of monocular deprivation (MD) in animals where the PNN had been degraded

- comparing visual processing in awake animals with animals anesthetized by the general anesthetic Midazolam, in both chABC injected and untreated animals.

This was performed using a novel approach combining microinjections of chABC with chronic multi-electrode recordings in awake and anesthetized animals.

2 Materials and methods

2.1 Approvals and research animals

The practical work in this study was done at the Department of Biosciences (IBV), Faculty of Mathematics and Natural sciences, University of Oslo, Norway. All experiments were approved by the Norwegian Animal Research Committee (FDU) prior to initiation. The housing and treatment of animals satisfy the criteria set by the European Union and the FDU. All participating parties hold an animal researcher certificate (FELASA C), as is required by the Norwegian Food Safety Authority (Mattilsynet).

Twenty five male Long Evans hooded rats (locally bred), 3-6 month of age, and weighing 400-600 g, were used. Eleven were injected with chABC and implanted with microdrives with electrodes for extracellular recordings, four were either injected with artificial cerebrospinal fluid (aCSF) or not injected, implanted with microdrives and used as electrophysiological controls and ten were injected with chABC and used for histology. Of the animals injected with chABC and implanted with microdrives, four were injected with chABC in both hemispheres and underwent monocular deprivation (MD) for 5 days; they were subjected to visual stimuli and recorded from daily before and during the MD period. Seven were injected with chABC in one hemisphere, subjected to visual stimuli and recorded from daily for 10-15 days. Similarly, of the four animals injected with aCSF and implanted with microdrives, two underwent MD for 5 days and were subjected to visual stimuli and recorded from daily before and during the MD period, while the remaining two were subjected to visual stimuli and recorded from for 15-20 days.

The animals were housed on a 12h light/dark cycle, with lights on from 10:00 p.m. to 10:00 a.m. Rats are nocturnal animals, and all recordings were therefore performed in the dark phase. The temperature in the housing quarter was kept at 21±0.1°C, with a humidity level of 55±10%. The rooms maintained a ventilation rate of 5-20 times per hour and the light intensity in the light phase was >100 lux. Animals were initially housed three to four per cage with ad libitum access to food and water. They were kept

in polycarbonate cages (35x55x19 cm) with woodchip bedding from Scanbur A/S with plastic toys. In order to minimize the risk of injury to the animal and to the microdrives after surgery, animals were housed individually in larger transparent plexiglass cages (35x55x30 cm). They had ad libitum access to water, and were given 6-10 food pellets per 24 hours which maintained body weight during the experimental period, in addition to chocolate treats given as rewards.

2.2 Surgery preparations

2.2.1 Intracortical injections of chABC and aCSF

Glass pipettes were pulled from 1.2 mm (outer diameter) borosilicate capillary glass (Sutter Instrument Company, CA, USA), using a P-30 pipette puller (Sutter Instrument Company, CA, USA). Pipettes with several different tip diameters were tested; if the tips were too big (>40 µm) the pipette failed to penetrate dura mater, if the tips were too small (<10 µm) the pipette clogged after one or two tissue penetrations. Furthermore, to prevent tissue damage during the deep injections (750 µm below dura mater in the dorsoventral plane), taper length was also taken into account. I found the optimal pipettes to have a taper of 5 mm, and a tip with 15-20 µm opening diameter. To generate pipettes fulfilling these measurements, the “kimwipe method” (Oesterle, 2011) was used. The pipette tips after pulling had an opening diameter of 1-5 µm and a taper length of 1 cm; the optimal opening and shape were obtained by running the pipette once through a “Kimwipe” paper towel. Pipettes were then backfilled with mineral oil and assembled into a NanoJect II (Drummond Scientific Company, PA, USA) micro injector, and loaded with chABC or aCSF.

Protease free Chondroitinase ABC (chABC) from *Proteus vulagaris* was purchased from Seikagaku (Tokyo, Japan) in 2U vials and from Amsbio (Abingdon, UK) in 10U vials, and diluted in phosphate-buffered saline (PBS) to aliquots of 61 U/ml, which were stored at -20°. In order to visualize the injections, aliquots were further diluted with Fast Green FCF (Sigma-Aldrich Chemie, Munich, Germany) just before pipette loading, to a final concentration of 48 U/ml, in accordance with Pizzorusso (2002).

The aCSF was purchased from Harvard apparatus (Massachusetts, USA) and mixed with Fast Green FCF in a 4:1 ratio.

2.2.2 Tetrode and microdrive assembly

Tetrodes were constructed from 17 µm-diameter platinum-iridium wire (California Fine Wire Company, CA, USA) by creating a loop from a single piece of wire with a small piece of tape; the wire was then placed over a magnetic stirrer and twisted to make two loops. A stir bar was hung at the bottom of the loops in such a manner that, when the magnetic stirrer was turned on, the four pieces of wire making up the loops were twisted around each other. When the wires were intertwined, they were heated to fuse by a heat gun for approx. 30 seconds, and the ends cut free. This gave the tetrode a more rigid structure. The heavy polyimide enamel insulation was removed at the outermost tips by holding the four free ends over a lighter flame for 0.5 second, to complete the tetrode. Four such tetrodes were assembled in a microdrive (Axona Ltd, Herts, UK) and secured with conductive silver paint (HK Wentworth, Leicestershire, UK) and several layers of nail varnish to protect the electrodes from mechanical damage. In order to obtain less resistance and thus enhance the sensitivity of the electrodes, the impedance of each electrode was lowered from around 1500 kΩ to 150-250 kΩ by electroplating them in a platinum solution (Ferguson et al., 2009).

2.3 Surgical procedures

All animals were anaesthetized with isoflurane (Baxter, Oslo, Norway) mixed with air, at a constant flow of 2L/min. Anesthesia was induced at a concentration of 5% isoflurane, which was gradually lowered to 1-2.5% during the operation. After anesthesia was induced, the animals' heads were immobilized in a stereotaxic frame (World Precision Instruments Ltd, Hertfordshire, UK) by positioning ear bars in the external auditory meatus, and the midline of the skull aligned with the frame to facilitate stereotaxic measurement of coordinates, according to the atlas of the rat brain by Watson and Paxinos (George Paxinos, 2007). The flat skull position was obtained by the use of a height-adjustable nose-clamp. The animals were given subcutaneous (s.c.) injections of Temgesic (buprenorphine, 0.04 mg/kg), Convenia (cefovecin

sodium, 8 mg/kg) and penicillin G (13.2 mg/kg), in addition to local s.c. injections of Marcain adrenalin (bupivacaine; adrenalin, 1mg/kg) in the scalp before surgery began. Heart rate, breathing rate, blood O_2 saturation and core temperature, the latter in a feedback mechanism connected to a heating pad, were continuously monitored throughout the operation, through a MouseStat system (Kent Scientific, CT, USA). In addition, the hind paw withdrawal reflex was used to assess the depth of anesthesia.

In order to minimize the risk of infections, surgery procedures were kept aseptic. All equipment was heat sterilized (150°C for 90 minutes) or autoclaved (cotton swabs) before surgery. An area spanning from between the eyes to just behind the ears was shaved and cleaned with ethanol, chlorhexidine and iodine solution (2%). A longitudinal cut was made in the skin, and skin and muscle tissue moved aside with artery clamps to expose the skull. The skull was constantly kept moist throughout the operation with sterile saline water (0.9% NaCl) to prevent the skull bones from drying out, and to reduce heat damage during drilling. Coordinates for injection and recording sites were measured in relation to bregma and lambda (skull landmarks at the intersections of the sagittal and coronal, and sagittal and lambdoidal skull sutures, respectively). Craniectomies of 2.5 mm diameter were performed bilaterally using a hand-held Perfecta-300 dental drill (W & H Nordic, Täby, Sweden). In addition, holes were drilled for grounding and stabilization of the implants: four jewelers' screws were attached anterior to bregma and three were attached posterior to lambda. Two of the former, one in each hemisphere, rested on the cortex and were connected to a microdrive as grounding after microdrive implant (figure 2.1).

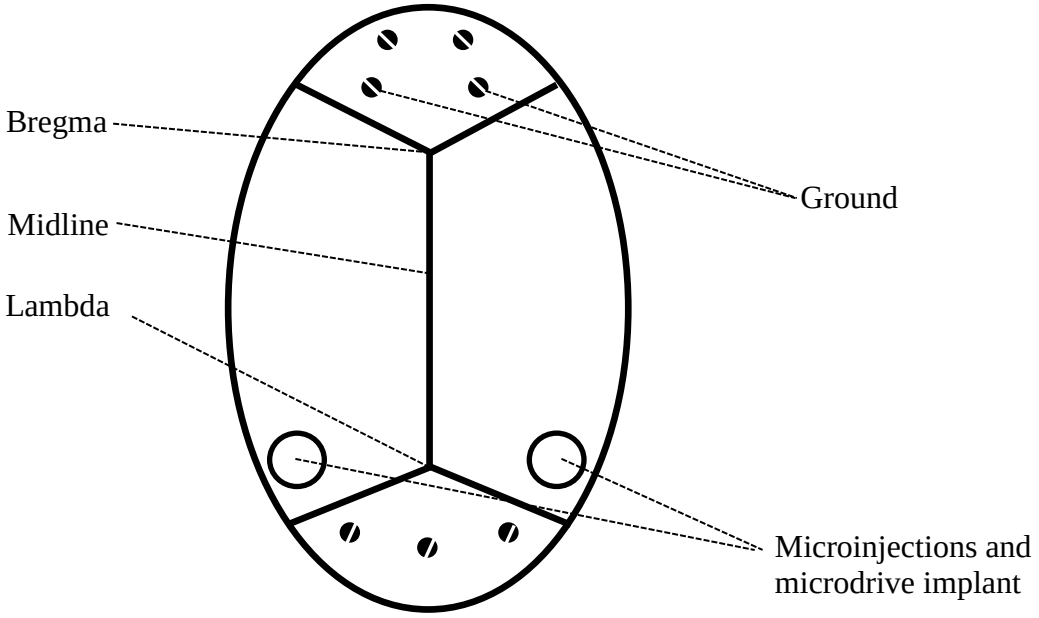

Figure 2.1: Overview of the exposed scull and craniectomies. Four screws were attached in the anterior part of the exposed scull, two for grounding and two for stabilization, and three screws were attached in the posterior part for further stabilization of the implant. Craniectomies were performed bilaterally for chABC/aCSF injections and microdrive implant.

2.3.1 Microinjections

The micro injector was mounted to the stereotaxic frame, and injections made at five sites within the visual cortex in each hemisphere; at each site the injections were made at two depths to ensure optimal coverage. In addition, to prevent saturation and mechanical damage of the tissue, the injections at each position were performed as 41 single injections of 9.2 nL each, making a total volume of 377 nL, injected over two minutes, at each position. Injection coordinates are listed in table 2.1.

Table 2.1: Coordinates for injections of chABC and aCSF. AP: anterioposterior ML: mediolateral DV: dorsoventral. AP and ML distances are relative to lambda and the midline, respectively.

AP	ML	DV	Volume
Lambda + 1 mm	3.8 mm	0.4 mm	377 nL
Lambda + 1 mm	3.8 mm	0.8 mm	377 nL
Lambda – 1 mm	3.8 mm	0.4 mm	377 nL
Lambda – 1 mm	3.8 mm	0.8 mm	377 nL
Lambda	4.6 mm	0.4 mm	377 nL
Lambda	4.6 mm	0.8 mm	377 nL
Lambda + 1 mm	5.4 mm	0.4 mm	377 nL
Lambda + 1 mm	5.4 mm	0.8 mm	377 nL
Lambda – 1 mm	5.4 mm	0.4 mm	377 nL
Lambda – 1 mm	5.4 mm	0.8 mm	377 nL
Total			3.77 µL

2.3.2 Microdrive implants

Microdrives were implanted in the binocular region of the primary visual cortex, at the following coordinates:

AP: lambda ML: 4.7 mm DV: 0.3 mm

First, a small area of dura was removed; the microdrives were mounted to a holder and attached to a stereotaxic tower on the frame and lowered into position. An outer cannula protecting the tetrodes was slid down to rest on the dura. Next, the ground cables of the microdrives were soldered onto the ground cables attached to screws, and

the holes were covered with dental Spongostan (Ethicon, Norderstedt, Germany) to protect the brain from the wet dental acrylic cement. Finally, the microdrives were secured with a 0.5-1 cm thick layer of dental cement. The antibiotic ointment Fucidin was applied at the edge of the wound at the end of the operation to prevent bacterial growth.

The exact coordinates in AP and ML planes did vary to a small extent (± 0.2 mm), due to variations in positions of blood vessels in the cortex, which have to be avoided at tetrode lowering. In addition, the tetrodes were moved in the DV plane during the recording period (the microdrive allows the tetrodes to be moved stepwise in the DV plane, where one full turn of the screw is equal to an increment of 200 µm). The two microdrives and the dental cement used to secure them weighs a total of approximately 7 grams, constituting 1.5-2 % of the body weight of an adult (500 g) rat.
All animals were given s.c. injections of Rimadyl (carprofen 5mg/kg) at the end of the operation. Furthermore, the animals were given s.c. injections of Rimadyl (carprofen 5mg/kg) and Penicillin G (13.2mg/kg) the three following days. In the event of a suspected infection, Fucidin ointment was applied at the edge of the wound.

Animals without microdrive implant (histology controls) were injected as described above, and the hole filled with KWIK-SIL silicone (World Precision Instruments Ltd, Hertfordshire, UK). The wound was cleaned with 0.9% NaCl and 96% ethanol, and sutured shut with 10-15 stitches. Fucidin ointment was applied around the edge of the wound. Post-operative medication procedures were identical to those described above.

For animals that underwent MD, this was initiated after electrophysiological measurements had started. The MD animals were anesthetized by an s.c. injection of a 1:1 mixture of Hypnorm/Midazolam (Fentanyl; Fluanizone; 0.08 mg/kg; 2.5 mg/kg, Midazolam; 0.25mg/kg). After recording visual responses, anesthesia was topped off with ¼ of the initial dose, and one of the eyes sutured shut with 4-5 stitches. Fucidin ointment was applied daily. After five days, the animals were again anesthetized with Hypnorm/Midazolam, and the suture removed. Visual responses were recorded, and the animals were then given an intraperitoneal overdose of Equithesin and sacrificed in order to perform histological experiments, as described below.

2.4 Electrophysiological recordings

All recordings, unless described otherwise, were performed in awake, freely behaving animals. The animals were divided into the following regimes:

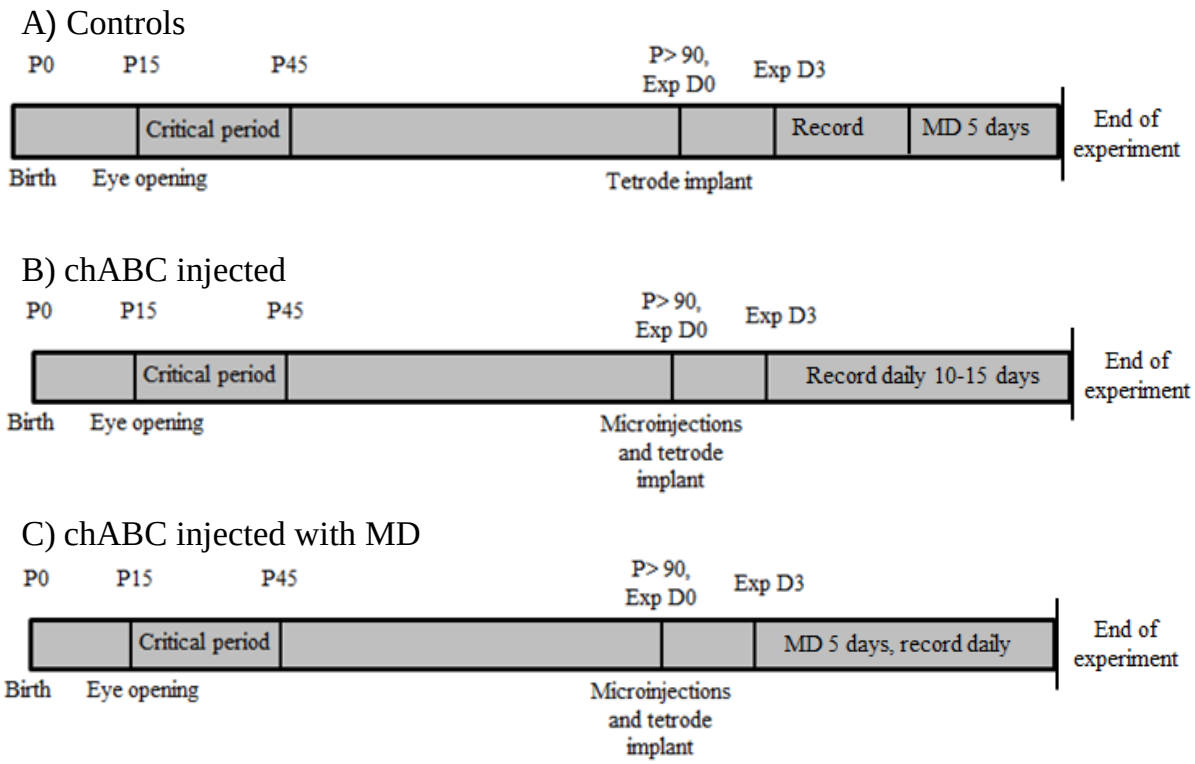

Figure 2.2: Different experimental regimes for the different animal groups. P= postnatal, Exp D=experimental day **A)** The control animals (n=4) were implanted with tetrodes, and from day 3 recorded from for a period of 10-15 days. During this period, two of them underwent MD for five days. **B)** The animals with chABC injections in one hemisphere and aCSF injections on the other (n=7) were injected and implanted with tetrodes, then recorded from daily for 10-15 days. **C)** The chABC injected animals that underwent MD (n=4). They were injected and implanted with tetrodes, and underwent MD for 5 days; neuronal activity was recorded daily.

2.4.1 Recording setup

To allow the animal to recover fully from surgery, electrophysiological recordings were not initiated until three days after surgery. Before each recording session, the rats rested on a towel in a large flower pot on a pedestal. The animals were connected to the recording equipment and placed in a 25x25x35 cm glass box, surrounded by four 17” computer monitors (Dell Computers, Limerick, Ireland). If the signal was “silent”, i.e. no cells were active, the tetrodes were lowered by 50µm, and the animal connected again later in the day. They were presented with visual stimuli during every recording.

The recording system used was daqUSB, provided by Axona (Herts, UK). Microdrives, each carrying 16 electrodes, were connected to a multichannel head stage. The head stage was coupled, through a lightweight multi-wire cable, to a pre-amplifier, which was again connected to the 32-channel recording unit. The Axona system also provides a digital amplifier in the recording software. Both analogue and digital amplifiers were used in all the experiments. A counter-weight system was installed in order to relieve the extra weight of the cables and head-stage from the animal, so as to allow the animal to move freely inside the box. Data collection started when the signal amplitudes exceeded 4-5 times the noise level. Signals were amplified 10000-15000 times and band-pass filtered between 0.8 and 6.7 kHz. Triggered spikes were stored to disk at 48 kHz (50 samples per waveform, 8 bits/sample) with a 32-bit time stamp (clock rate at 96 kHz). Spike waveforms above a threshold of 50 µV were time-stamped and digitized at 32 kHz for 1 ms, and saved to the hard-drive for offline analysis. One of the 16 channels in each hemisphere was used to record EEG; EEG signals were amplified between 3000 to 5000 times, lowpass-filtered at 500 Hz and stored at 4.8 kHz (16 bits/sample).

The computers used to generate the visual stimuli and electrophysiological recordings were connected, to allow for synchronized time-stamping of stimuli and spikes.

2.4.2 Visual stimulation and monocular deprivation

At every recording session, the animals were subjected to visual stimulation; during the first days of recording in order to identify visually modulated neurons during recordings, and eventually to determine orientation tuning and ocular dominance properties of the cells. Visual stimulus was generated in Matlab using the Psychophysics Toolbox extensions (Brainard, 1997), and consisted of drifting gratings or bars in 4 or 8 orientations, both with a spatial frequency of 0.08 cycles per degree of visual angle, which is the preferred spatial frequency of rodent visual cortical neurons (Girman et al., 1999; Niell and Stryker, 2008). The different orientations were presented for three seconds, in 12 or 24 repetitions each in random order, with a grey screen presented in between the stimulations. For every stimulus event, a time-stamped log file was created to allow for stimulus-response analysis.

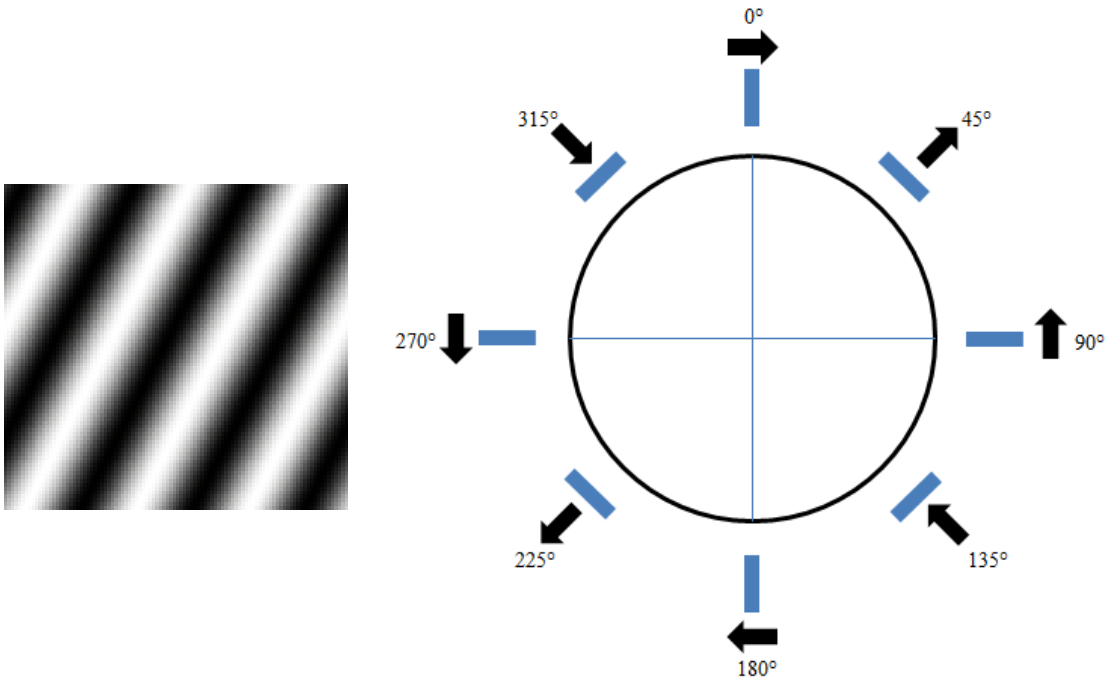

Figure 2.3: Visual stimulation was done with drifting gratings (left) and drifting bars (not shown), presented in 4 or 8 orientations. Stimulation was presented for three seconds each in 12 or 24 repetitions, with a grey screen displayed between each presented orientation.

The stimuli presented during daily awake recordings were:

1. Drifting gratings; 4 orientations in random order; 24 repetitions (6:30 min)
2. Drifting bars; 8 orientations in random order; 12 repetitions (7:30 min)
3. Drifting bars; 8 orientations in random order; 12 repetitions (7:30 min)
4. Drifting gratings; 4 orientations in random order; 24 repetitions (6:30 min)

When stable cells were recorded over several sessions (1-2 days), the stimulus regime was changed, in order to determine orientation tuning and OD properties. Animals were initially presented with a series of stimuli while awake (see below), before they were anaesthetized by an s.c. injection of a 1:1 Hypnorm/Midazolam mix (Fentanyl; Fluanizone; 0.08 mg/kg; 2.5 mg/kg, Midazolam; 0.25mg/kg). The anaesthetized animal was placed on a heating pad in front of a computer monitor with their eyes 25 cm from the screen which is sufficient to cover the entire visual field, and displayed various stimuli while alternating covering of one of the eyes. The sequence of stimuli displayed during these sessions was:

1. Drifting gratings; 4 orientations in random order; 24 repetitions (6:30 min)
2. Drifting bars; 8 orientations in random order; 12 repetitions (7:30 min)
3. Drifting gratings; 8 orientations in random order; 12 repetitions (7:30 min)

The animal was then anesthetized and presented with the following stimulation paradigm:

1. Drifting bars; 8 orientations in random order; 12 repetitions (7:30 min)
2. Drifting gratings; 8 orientations in random order; 12 repetitions (7:30 min)
3. Drifting gratings; 4 orientations in random order; 12 repetitions (3:30 min); left eye closed
4. Drifting gratings; 4 orientations in random order; 12 repetitions (3:30 min); right eye closed
5. Drifting gratings; 4 orientations in random order; 12 repetitions (3:30 min); right eye closed
6. Drifting gratings; 4 orientations in random order; 12 repetitions (3:30 min); left eye closed
7. Drifting bars; 8 orientations in random order; 12 repetitions (7:30 min)
8. Drifting gratings; 8 orientations in random order; 12 repetitions (7:30 min)

In animals that underwent MD, one of the eyes was then sutured shut with 4-5 stitches and the animals were left to recover in their cages until the next day. Which eye was shut was selected based on which hemisphere had the highest number of recorded neurons; the contralateral eye to this side was chosen in order to maximize the chances of recording from several cells over several sessions. The former sequence of stimuli was repeated every 24 h for five days, and the suture monitored closely to make sure no light was entering the eye. After five days, the suture was removed, and the latter stimulus sequence, including those with the animal under anesthesia, was repeated. Animals which did not undergo MD were left to recover in their cages after anesthesia sessions, and recorded from again the next day while awake, with the former stimulus sequence.

2.5 Histology

Before sacrifice, all rats were given an intraperitoneal overdose of Equithesin (chloral hydrate; magnesium sulfate; pentobarbital sodium; propylene glycol; 105mg/kg; 52.5 mg/kg; 25 mg/kg; 105 mg/kg). When deeply anesthetized, the animal was transcardially perfused with 0.9% NaCl, followed by 4% paraformaldehyde (PFA) in PBS. The brains were dissected out and post-fixed in PFA for a minimum of 24 hours, then incubated for three days at 4°C in a 30% sucrose solution. They were flash-frozen and cut into 40µm thick coronal sections using a cryostat (Ortomedic, Lysaker, Norway), and collected at Superfrost plus glass slides (Thermo Fisher Scientific, Oslo, Norway), or collected with a fine paint brush and put in PBS for immunohistochemistry staining. Complete protocols for the staining procedures are found in Appendix (chapter 5.2 and 5.3).

2.5.1 Immunohistochemistry staining for PNNs

Staining for PNNs was performed on free-floating sections; one section every 80 µm across the visual cortex was collected, with a total of 15-20 sections per animal. Sections were blocked in TS-PBS and incubated at 4°C overnight in a 1/200 dilution of the primary antibody, biotin-conjugated agglutinin from *Wisteria floribunda* (WFA) (Sigma-Aldrich Chemie, Munich, Germany). On the second day, endogenous peroxidase activity was quenched by a 1.5% H_2O_2-solution, sections incubated with biotinylated *Horse radish* peroxidase, and an avidin-biotin complex staining solution (Thermo Fisher Scientific, Oslo, Norway). Staining was visualized by adding 3,3'-Diaminobenzidine (DAB) solution (DAB pellets purchased from Sigma-Aldrich Chemie, Munich, Germany), and the reaction stopped by immersing sections in TNS. The sections were mounted to Superfrost plus glass slides (Thermo Fisher Scientific, Oslo, Norway), and dried at 37°C. Finally, the sections were dehydrated with ethanol and xylene in 70%, 80%, 90%, 95%, and 100% ethanol and xylene, respectively, and secured by a cover slip with Entellan (Merck Millipore, Darmstadt, Germany) or distilled water, depending on whether the animal was used only for histology or for histology and electrophysiological recordings.

2.5.2 Nissl staining

To verify recording positions of the tetrodes, sections were stained for Nissl bodies. The sections were hydrated in dH_2O and immersed in Cresyl Violet staining solution, gradually dehydrated as described above, secured with a cover slip with Entellan, and closely investigated under a microscope. An estimated shrinkage of 10% which happens during the perfusion and fixation period was accounted for when assessing tetrode depth in sections, relative to the natural state.

2.5.3 Immunohistochemistry staining for glia reactivity

Staining for glia cells was performed on free-floating sections. Sections were blocked in TS-PBS and incubated overnight at 4°C in a 1/500 dilution of the primary antibody, rabbit anti glial fibrillary acidic protein (Dako Cytomation, Glostrup, Denmark). On the second day, endogenous peroxidase activity was quenched by a 2.5% H_2O_2 solution. The remainder of the protocol was identic to that described in chapter 2.5.1.

2.6 Data analysis

2.6.1 Photo acquisition and analysis

Stained sections were photographed using two different setups. Sections used for histological assessment of PNN regeneration were photographed using an Axiocam HRZ camera (Carl Zeiss, Oberkochen, Germany) through an Axioplan 2 microscope (Carl Zeiss, Oberkochen, Germany). High-resolution images were then stitched together using the MosaiX module in the AxioVision software (Carl Zeiss, Oberkochen, Germany). Sections stained for PNNs and due for Nissl staining were photographed using a Nikon Coolpix 995 camera (Nikon Nordic, Fornebu, Norway) through a Leica Wild MZ8 microscope (Leica microsystems, Wetzlar, Germany). After Nissl staining, the section containing the tetrode tracks were processed as described with the former setup.

Images were cropped using Adobe Photoshop CS2 (Adobe, California. USA). To measure regeneration of PNNs, greyscale value measurement in ImageJ (NIH) was used. The images were inverted relative to an 8-bit color scale (255 grey shades, each

assigned an intensity value). An area of 1x1 mm was selected in the approximate middle region of the injected area, i.e. the binocular part of V1, and the mean greyscale value compared to a 1x1 mm area in the same region in the other hemisphere of the same section to give the ratio injected : control. In sections with bilateral injections, the control measurement was made immediately adjacent to the injected area. At time-points where there were sections from more than one animal, the mean ratio value was used.

2.6.2 Spike sorting

Spike sorting was performed manually using the graphical cluster-cutting software Tint (Axona Ltd, Herts, UK). The cluster-cutting method uses two-dimensional scatter-plots based on the waveform amplitudes of single spikes from each of the single units in a tetrode. Spikes from single cells tend to form distinguishable clusters separated from the noise, and these were enclosed with a boundary. Care was taken to ensure that no spikes were left out, and that any noise within the cluster was removed before analysis. In addition, cross-correlation analysis was performed to ensure that the boundaries were correct: if the lag period between spikes within a cluster was shorter than 1 ms, the cluster was presumed to contain spikes from more than one cell, and the spikes sorted accordingly. Cells that were difficult to isolate with high precision ($n>70$ for both controls and chABC) were left out of the analysis. An example of a cutting window is shown in figure 2.4.

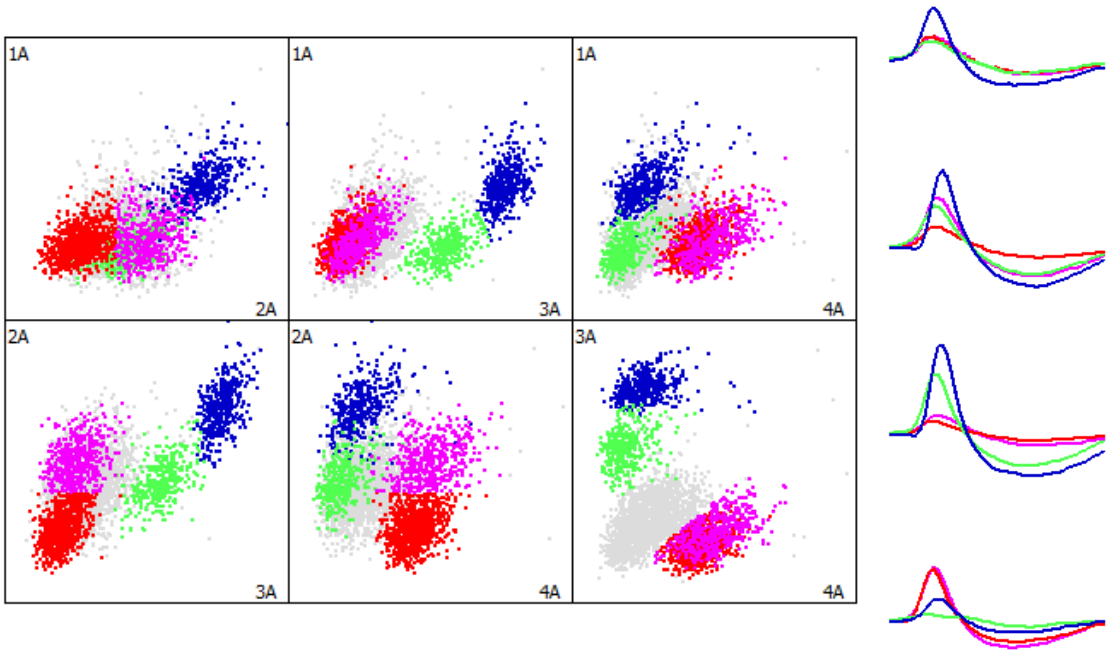

Figure 2.4: Spike sorting in Tint. Spikes from the same cell are registered differently on all electrodes. Single spikes' amplitude on each electrode (1A - 4A) is measured and plotted in scatter plots (left). These tend to form clusters separated from the noise, and are enclosed with a boundary, which is color coded. Mean waveforms of the 4 clusters labeled are shown to the right.

Cells were then further classified as inhibitory interneurons and excitatory pyramidal cells using the Matlab program AxWaveForm 2.1 (R. Skjerpeng, NTNU, Trondheim, Norway and T. Hafting, University of Oslo, Oslo, Norway) (figure 2.5 A and B). The program uses .cut-files from the cluster-cutting software as input files, and measures several parameters from the average waveform in each cluster at each single unit on the tetrode, such as duration in time from wave peak to wave trough, wave peak to baseline and wave amplitude. Output values of these measurements were in Microsoft Excel format, and were analyzed by testing different values of the population against each other. The model that gave the clearest and most accurate separation was when cells were separated based on peak to trough duration and the ratio between peak to baseline duration and baseline to trough duration (figure 2.5) (Csicsvari et al., 1999).

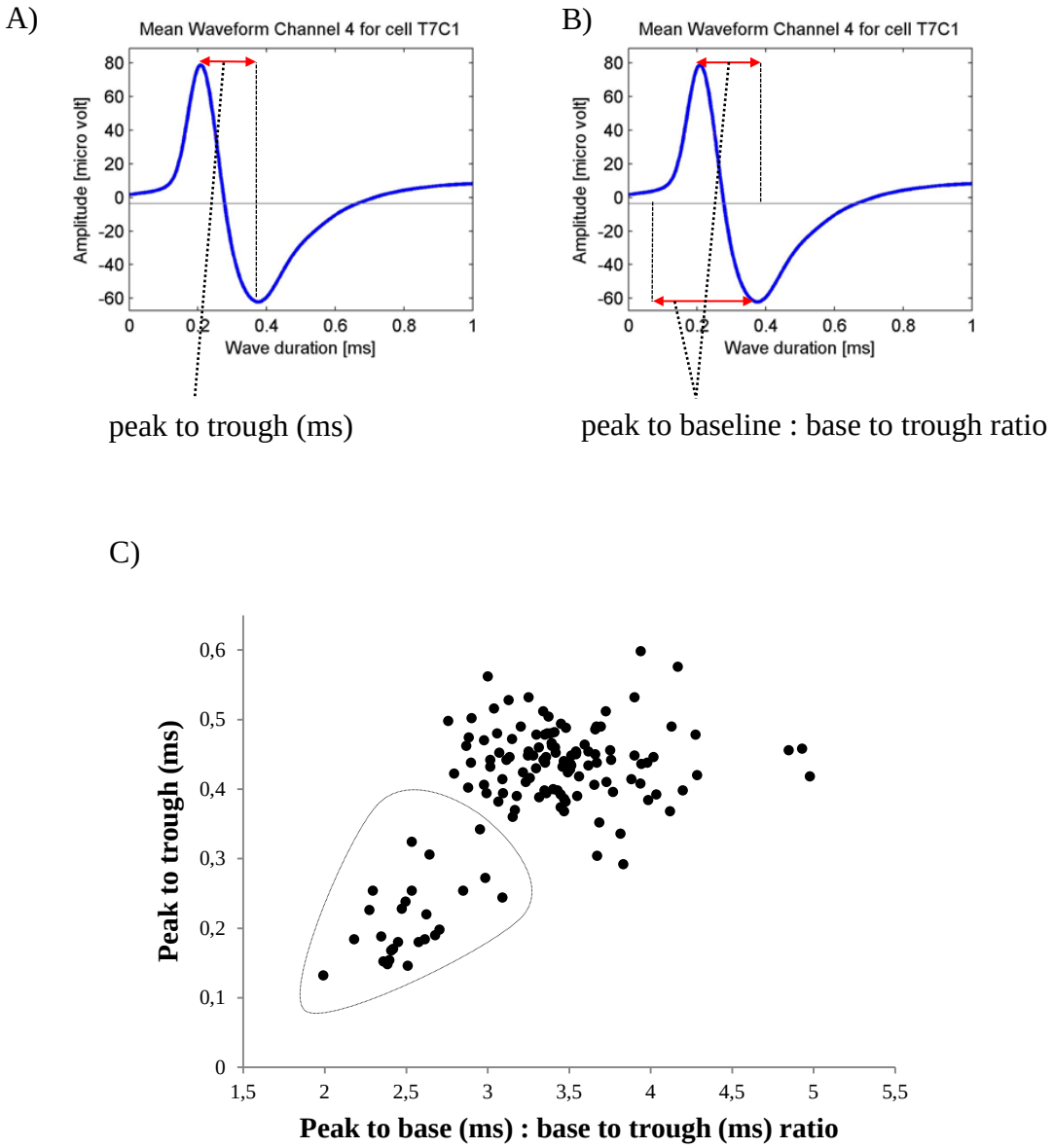

Figure 2.5: Classification of cells into inhibitory and excitatory neurons. Cells were separated based on peak to trough time (**A**) and the ratio between peak to base and base to trough time (**B**). Final classification is shown in **C**. 19% of cells were classified as inhibitory neurons.

2.6.3 Orientation tuning analysis

The tuning properties of cells were determined using custom MatLab software, which correlates the time-stamped log files from the visual stimulation to the time-stamped files of spikes sorted into clusters. The program generates a raster plot showing the coincidence of spikes from a given cluster to stimulation in the different presented

orientations, and line graph, or tuning curve, showing the average firing rate, in hertz, within the cluster in response to stimulation in the different orientations presented. An orientation selectivity index was calculated as the ratio in firing rate of (firing $\text{rate}_{\text{pref}}$ − firing $\text{rate}_{\text{orth}}$)/(firing $\text{rate}_{\text{pref}}$ + firing $\text{rate}_{\text{orth}}$), where firing $\text{rate}_{\text{orth}}$ was the mean response of the two directions orthogonal to the preferred direction (Wang et al., 2010).

2.6.4 Analysis of EEG

The local field potential (LFP) was recorded from both hemispheres in most of the recordings. These files were analyzed using two different approaches: power spectrum and wavelet analysis. The power analysis was performed using the Matlab program AxPowSpec (R. Skjerpeng, NTNU, Trondheim, Norway and T. Hafting, University of Oslo, Oslo, Norway) which gives the power, or abundance, of the frequencies within a defined frequency interval relative to each other, through the entire recording. The frequency interval used for most analysis was 1-130 Hz.

Wavelet analysis was performed in order to visualize changes in the EEG through the recording. This was also performed in Matlab, with the program FieldTrip (Oostenveld, Fries, Maris, Schoffelen, Radboud University Nijmegen, Nijmegen, Holland and E. Norheim, Norwegian University of Life Sciences, Ås, Norway). The program makes a spectrogram plot for a frequency interval over time, thus making it possible to look for changes in the LFP with high temporal resolution.

Because almost all of the recordings were done while the animals were awake, we investigated whether it is possible to determine specific properties of cells in awake, freely behaving rats. This was indeed the case, but the number of cells with a clear tuning preference was highly variable, and cells which did display tuning properties did not necessarily do this consistently though several recordings. If the animal is very active, variations of the angle of the head and side-to side movement will make it impossible to determine the specific tuning properties. However, if the animal is generally calm and not moving around a lot, it would be possible, as the stimulus is presented all around the animal. In an attempt to categorize recordings as “calm” or

"active", we tried to correlate the EEG to the actual activity of the animal: delta wave activity (1-4 Hz) is known to correlate with sleep and low level of physical activity (Steriade et al., 1993) while theta wave activity (6-12 Hz) correlates with walking and exploratory behavior (Whishaw and Vanderwolf, 1973). A modified version of AxPowSpec was used, AxThetaMod (T. Hafting, University of Oslo, Oslo, Norway), which compares the abundance of theta waves relative to delta waves during a recording. If the ratio shows a strong value towards one of the two, this should indicate whether the animal is calm or very active. To investigate whether this approach to classify recordings for tuning property analysis would be feasible, 15 random awake recordings were selected and analyzed. However, there was no correlation between the recordings which showed a high delta ratio and the ones where cells showed proper orientation tuning. Of all recordings in awake animals, less than 10% of the cells showed stable orientation tuning preference over several recordings. The tuning analysis, while clearly possible in awake animals, therefore only includes cells from recordings done in anaesthetized animals.

2.6.5 Statistical analysis

All statistical analysis were performed in Microsoft Excel 2010 (Microsoft, Washington, USA) and MatLab (Math Works, Massachusetts, USA), using the MatLab Statistics Toolbox. For between-group comparisons, firing rates were log transformed prior to testing. Samples were tested for normality and variance – none of the populations passed the normality test. Hence, all statistical testing was done using the Wilcoxon rank sum test (for testing between populations) and the Wilcoxon signed rank test (for testing within the same population). With regards to histology, the grey-scale values were normalized relative to the "day 3" control, and transformed to percentages. For awake/anesthesia analysis, a natural variation of 10% in firing rate was allowed for; cells where the change in firing rate from awake to anesthesia exceeded this were classified as "increased activity" or "decreased activity".

3 Results

The electrophysiology analyses in this study are based on data from 142 recorded neurons from 15 animals. Of these, 27 cells (19%) were classified as inhibitory neurons (see figure 2.5). Six animals underwent MD and the neurons recorded in these, during or after the MD period (38 cells), were treated separately and used only to study the effects of MD. In addition to these cells, >130 recorded cells were left out as they were difficult to isolate from each other, and background noise. A large majority (>80%) of the population of neurons was recorded between three and 12 days after surgery. Firing rates are shown in "box and whisker"-plots, as the display does not make any assumptions about the underlying distribution of the data and show the variation within a population, in addition to showing the median and standard deviation. The lower quartile includes the lower 25% of the population, while in the upper quartile, 75% of the data points are included. In the following box and whisker plots, outliers are denoted +, error bars indicate standard deviation, and ---- indicate median. In figure legends, SEM is short for standard error of the mean, and "n" refers to number of cells, unless mentioned otherwise.

3.1 Methodological assessment

3.1.1 The impact on cortical neurons of microinjections and tetrode implant

We chose to use glass pipettes to perform the injections of chABC, in order to minimize the damage to the cell layers we wanted to do electrophysiological recordings from. Furthermore, damage upon tetrode implant can destroy the tissue, and hence disturb the recordings. In order to investigate the mechanical damage applied by the injections and tetrode implant, sections were stained with WFA (to make sure the coordinates of the sections were the same as the injected area), and for Nissl bodies and glia cells. Upon damage to an area, glia cells will migrate and condense around the site (see chapter 1.2.3); this therefore provides a good measure of the damage inflicted. The Nissl stain labels cell bodies, allowing for the visualization of tetrode tracks; in addition to serving as a measure of damage, the recording positions needed to be verified. Sections were studied closely under a microscope, and the depths of the

tetrode tracks were measured. Recording positions were verified with an accuracy of ±100µm.

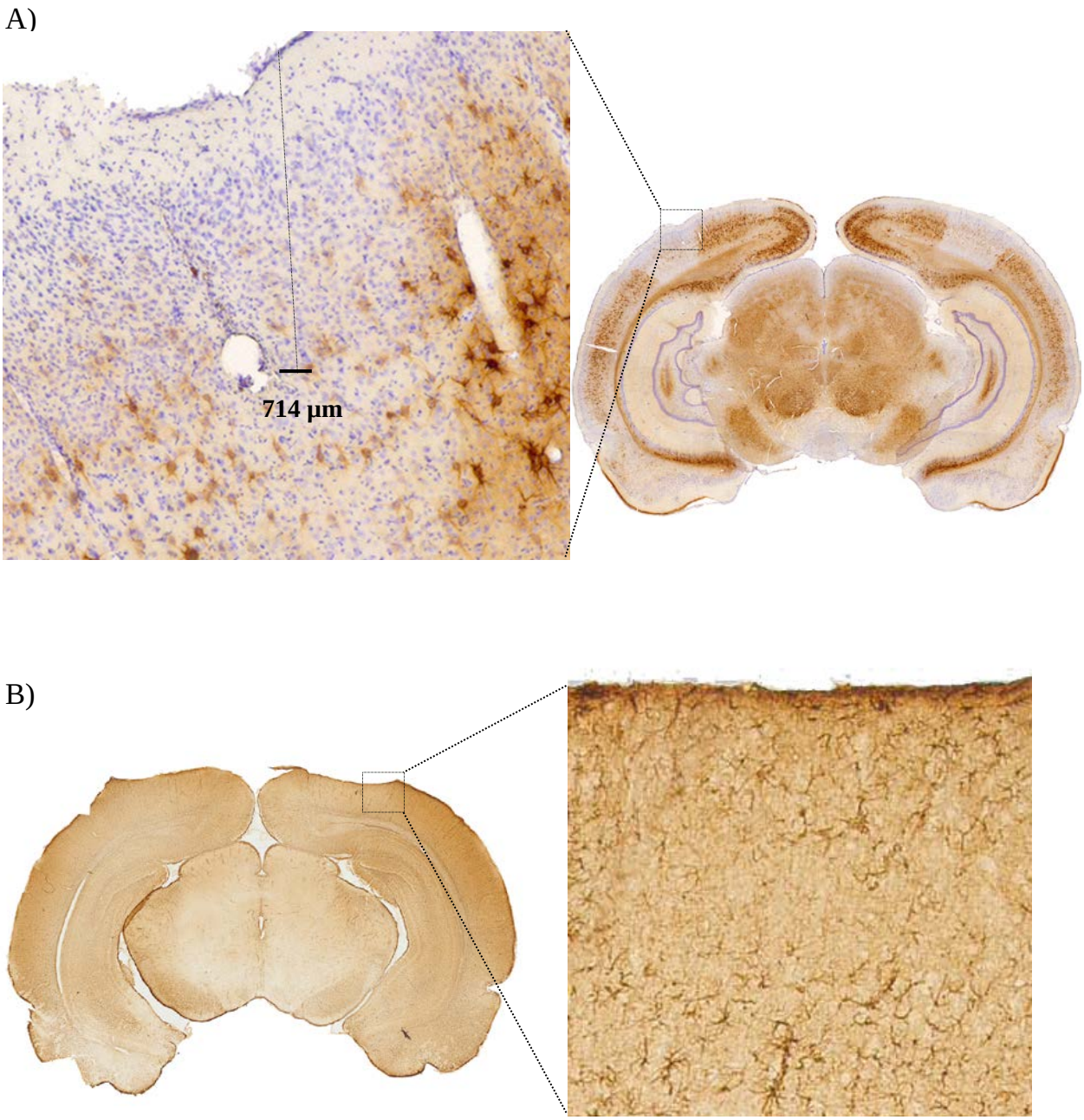

Figure 3.1: A tetrode track and microinjections in V1. The injections and tetrode implant leave very little damage to the cortex. **A)** A section stained with Wisteria floribunda agglutinin (WFA) and cresyl violet, in order to visualize PNNs and cell bodies, respectively. Staining of cell bodies verified recording positions with ±100µm. The tetrode track can be seen just to the left of the dotted line, as an irregularity in the cell bodies. Very little damage can be seen from the tetrode implantation, and the microinjections cannot be traced. **B)** A section stained with anti-glial fibrillary acidic protein (anti-GFAP), to visualize glia cells around the tetrodes, injections sites, and the tissue after PNNs were degraded. No glial response was observed.

The damage from the tetrode implant was fairly small (figure 3.1), although this did vary to some extent (additional tetrode tracks are shown in Appendix, chapter 5.4). The microinjections could not be traced with either staining procedure, indicating that the damage to cortical neurons from this procedure was minimal. Furthermore, the actual degradation of the PNN did not produce a glial response.

3.2 PNN regeneration

3.2.1 Regeneration of the PNN after enzymatic degradation

The enzyme chABC is efficient in digesting CS and thereby degrading PNNs, leading to alteration in plasticity (discussed in chapter 1.2.3). However, normal turnover of matrix proteins will eventually lead to reformation of matrix structures. The time-frame of this process is not known for the PNN structure. In order to determine a time-window for which to do electrophysiological recordings and sensory deprivation to investigate plasticity, animals were sacrificed at seven different time-points after chABC injection, and stained with WFA. The enzyme I used was very reliable, and the degradation was efficient in every injected animal (figure 3.2). This analysis was similar to that done by Brückner *et al.* (1998), but in my study, the animals were sacrificed at shorter intervals, as the most interesting period in relation to electrophysiological studies appeared to be a rather short period after chABC injection.

A) 3 days after chABC injection

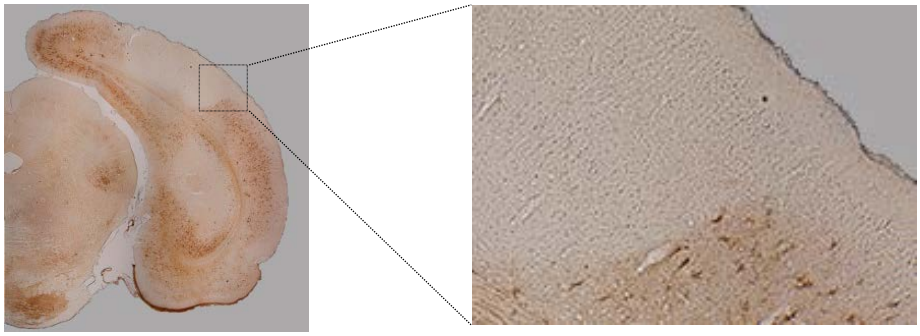

B) 10 days after chABC injection

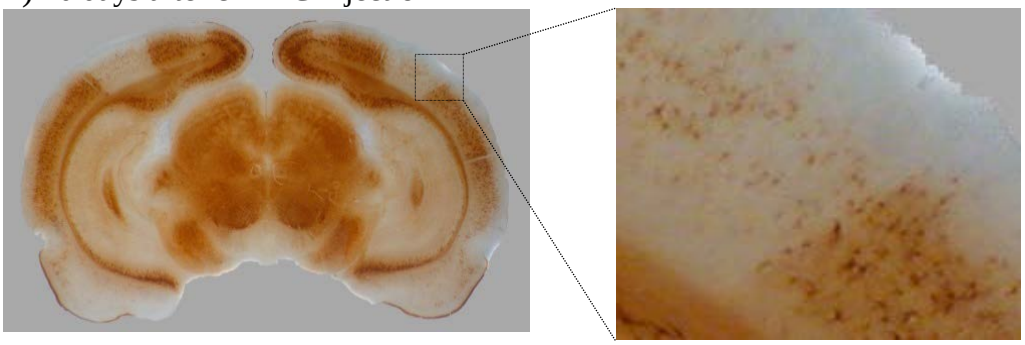

C) 14 days after chABC injection

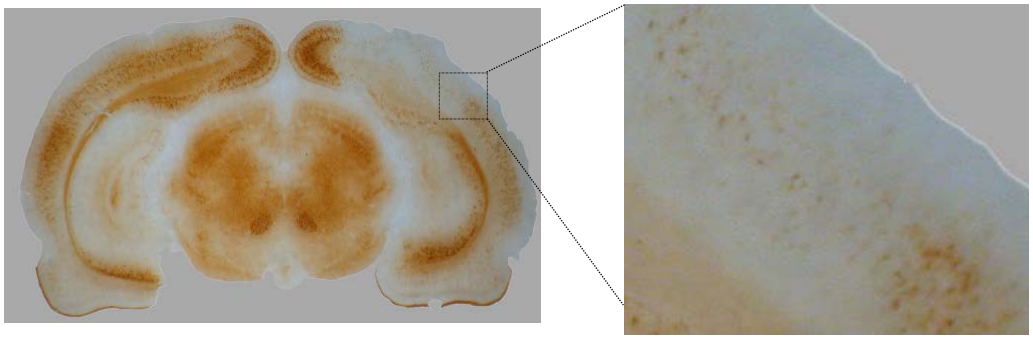

D) 17 days after chABC injection

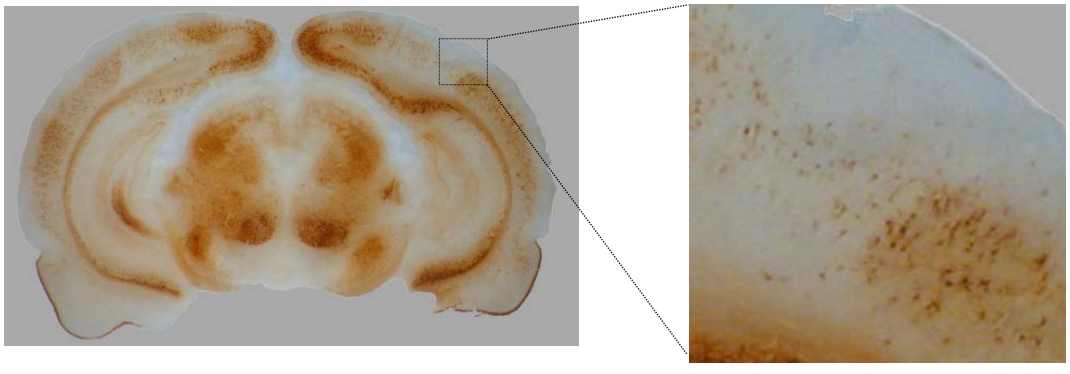

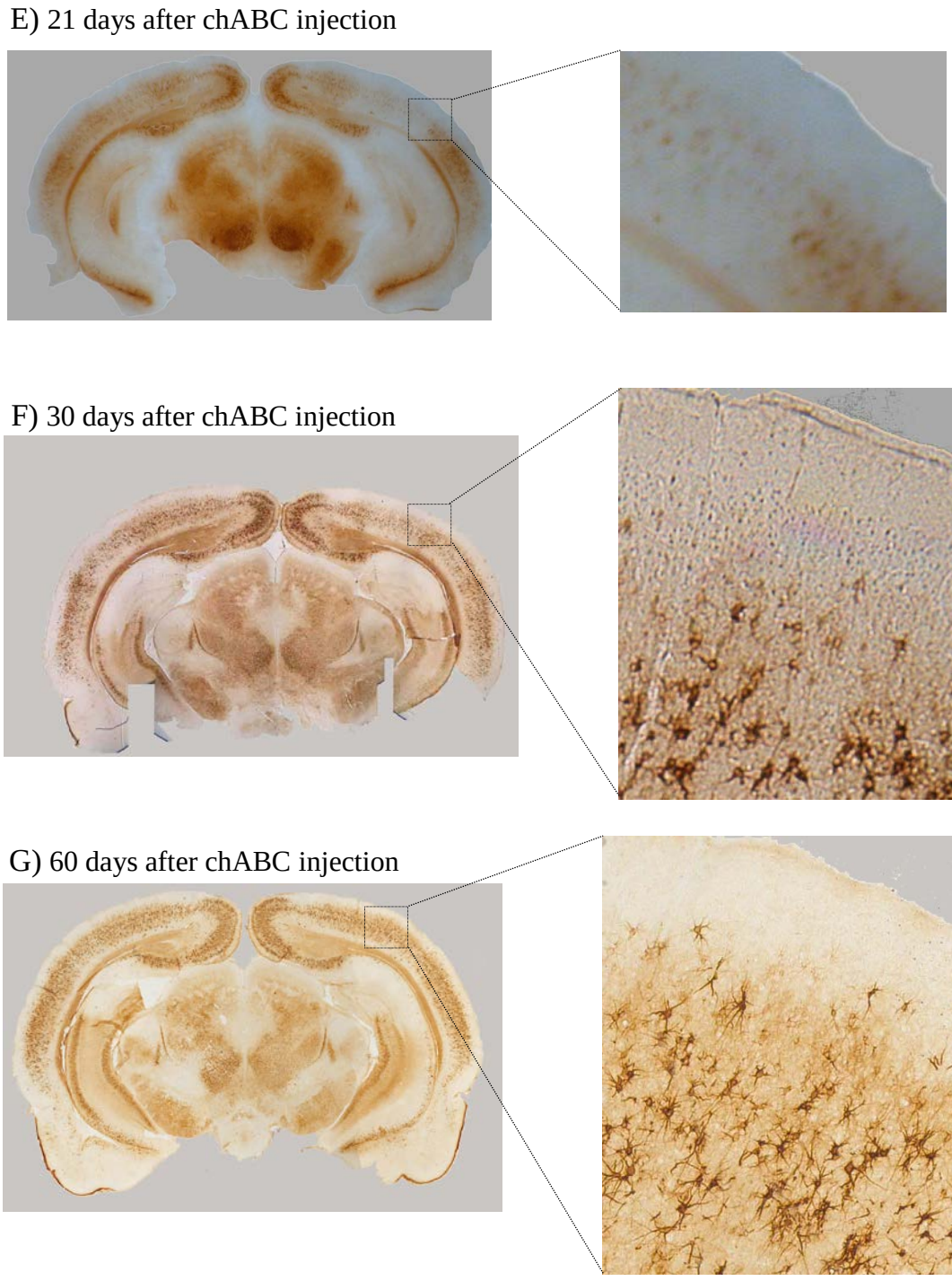

Figure 3.2: Regeneration of PNNs over time. Sections were stained with *Wisteria floribunda* agglutinin (WFA), which specifically labels the PNN. **A-G** shows sections from animals sacrificed 3, 10, 17, 21, 30 and 60 days after chABC injection, respectively. Images were acquired using two different microscopy set ups, hence the variation in quality.

In order to quantify the amount of labeling at the different time-points as a measure of PNN regeneration, the images were converted for greyscale intensity measure (see chapter 2.6.1). Sections were inverted relative to an 8-bit color scale (figure 3.3A). The

grey values of a 1 x 1 mm area within the injected area and a control area of 1 x 1 mm immediately adjacent, or the corresponding area in the other hemisphere, were compared. The ratio values were calculated by $chABC_{grey\ value}$: $control_{grey\ value}$, and converted to percentages. This was normalized relative to the ratio from three days after injection, as the WFA labeling showed that the PNN was completely degraded at this point (figure 3.2A). At two time-points (day 10 and 14 after chABC injection), sections used for electrophysiology were included; in these cases the mean ratio value from two animals were used. At the other time-points, only one animal was used.

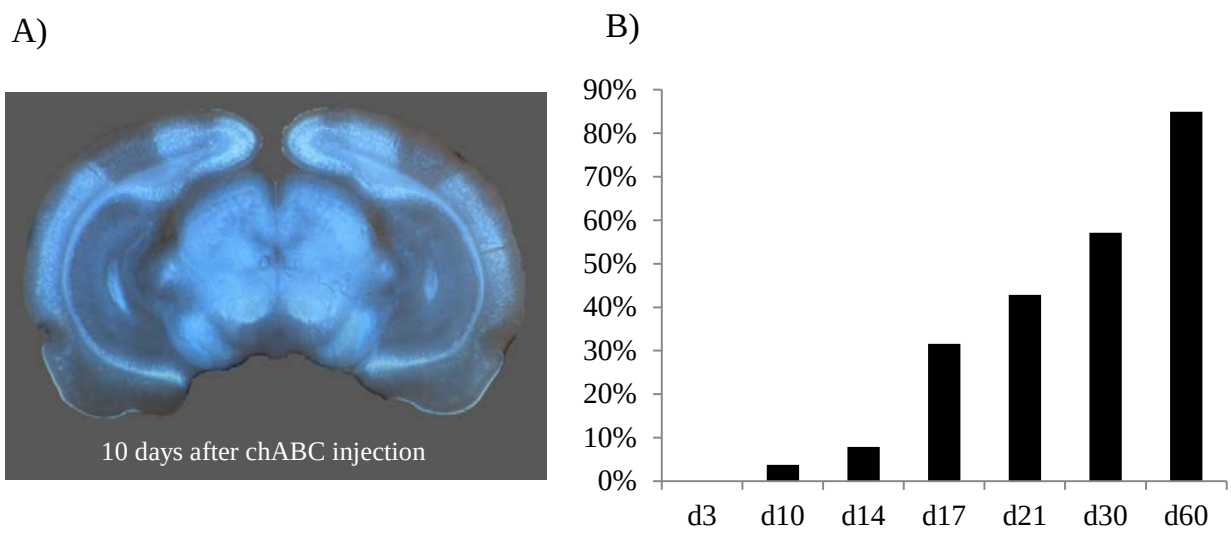

Figure 3.3: The reassembly of the PNN at different time-points after chABC injection was quantified using greyscale value measurements in ImageJ. **A)** Images were inverted relative to an 8-bit color scale. The section shown is from an animal sacrificed 10 days after chABC injection. **B)** The ratios between grayscale values were converted to percentages, where "3 days after injection" was set as 0% regenerated. n (animals)= 1 in each group, except at day 10 and 14, where n (animals)= 2. After 21 days, 43% was regenerated, while after 60 days, 85% was regenerated.

The analysis (figure 3.3B) showed that the PNN, or at least the part of it carrying the epitope for WFA, was regenerated gradually. There was a large increase between day 14 and day 17 (8% day 14, 31% day 17), possibly as a result of differences in tissue quality, and hence efficiency of the staining. In order to be sure that recordings were performed when the PNN was still largely degraded, all electrophysiological recordings were performed between three and 21 days after chABC injections. After 60 days, 85% of the PNN was regenerated.

3.3 The effects of PNN degradation on cortical processing

3.3.1 Cell stability after PNN degradation

The PNN has been proposed to form a major structural barrier in the CNS. The degradation of such a rigid structure could possibly open for increased cell motility, and increased axonal outgrowth. The tetrodes used for the electrophysiological measurements are stable in position and can record from the same cells over several sessions and days, and can thus be used to assess stability in position and activity of the same population of neurons. However, small movements of the tetrodes in relation to the tissue do occur, and it can be a challenge to record from the same neurons over time. I investigated if removal of PNNs influenced the overall stability of the tissue. This analysis depended on recording sessions where activity was recorded two or more days in succession, and with no change in the position of the tetrodes between sessions. Based on their waveform and position relative to each of the single electrodes on the tetrode (see chapter 2.6.2), and other cells recorded, cells were classified as the same cell as recorded the previous day, or a new cell (figure 3.4). In total, this resulted in 35 cells from three control animals and 60 cells from four chABC injected animals.

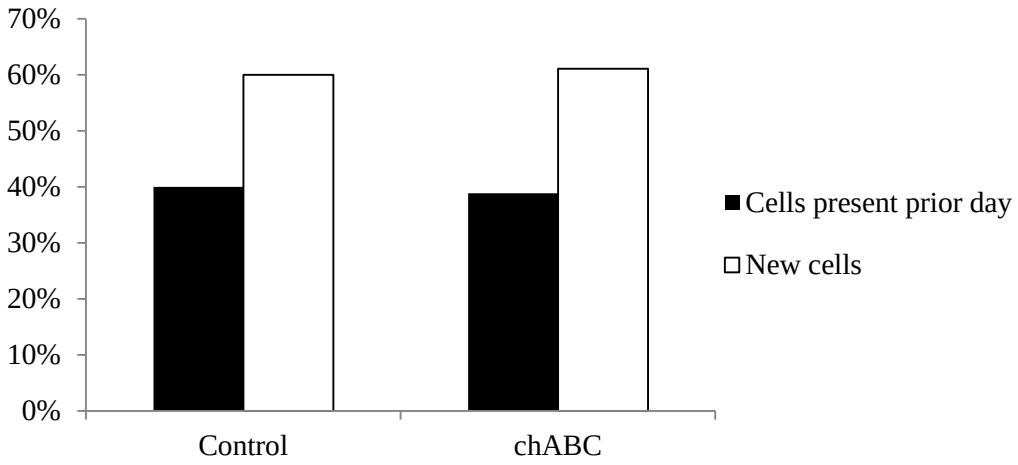

Figure 3.4: Cell stability in control and chABC-injected animals. Based on waveform and position in cluster space, cells were classified as "new" or "same as prior day" when comparing recordings in the same animal from two or more consecutive days. The position of the tetrodes was unaltered between the recordings used for the analysis. The difference between the groups was minimal, with control animals showing a 40:60 distribution, and chABC injected animals showing a 39:61 distribution. n (animals, cells) = 3, 35 (control) , 4, 60 (chABC).

The distributions in the groups were very similar (figure 3.4). For both control and chABC injected animals about 40% of the cells were recorded on consecutive days, while 60% of cells were new. This indicates that PNN degradation did not affect the stability of cells when considering cell motility. It does, however, show that in both control animals and chABC injected animals, there was a rather large “turnover” of cell populations. For every given day, approximately 60% of the cells were new to the population.

However, the stability of populations of cells can also be measured in the form of activity. I wanted to investigate whether the gradually reassembling PNN would affect the activity. As seen in figure 3.3B, after 10 days, the reassembly of the PNN has gradually started. Hence, I compared the activity of neurons at two time-points after injections and microdrive implant; one point where the PNN was completely degraded and at one point where the reassembly had begun. This was done by comparing firing rates of neurons when the animals were awake and being presented with visual stimuli. The size of the data set was affected by the fact that not all animals had measureable neuronal activity at every session. In order to increase population sizes, data from two days (day 3 and 4 after surgery, and day 9 and 10 after surgery) were pooled, to give populations of 20 (control day 3+4), 28 (chABC day 3+4), 13 (control day 9+10) and 28 (chABC day 9+10) cells, from four control animals and five chABC injected animals. Due to the large degree of substitution of the populations seen from day to day (figure 3.4), mainly new cells were included when pooling data from two consecutive days. Cells that were classified as inhibitory neurons, as described in chapter 2.6.2, generally showed a large variation in activity, with some cells having a firing rate several times higher than pyramidal cells. Including only a few inhibitory neurons could potentially skew the entire data set; hence, the analysis only included pyramidal neurons.

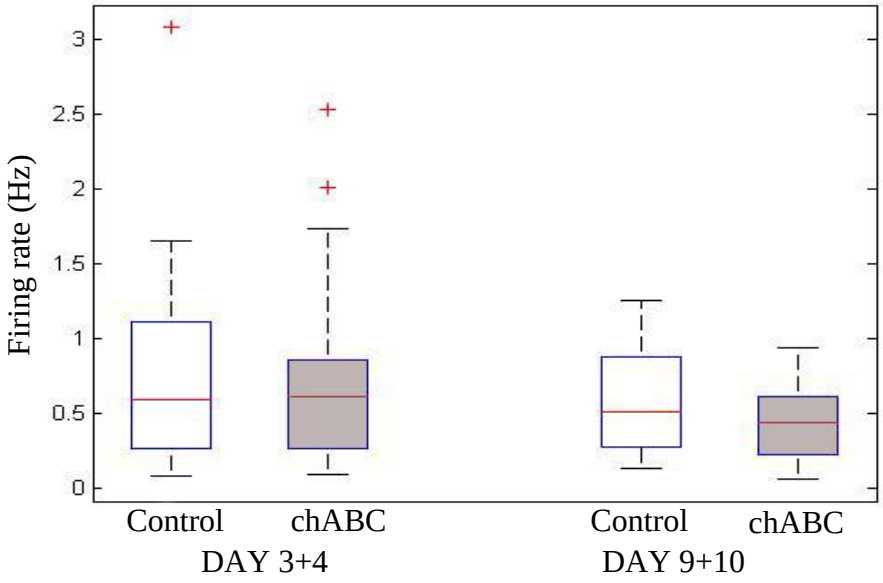

Figure 3.5: Firing rates of pyramidal cells recorded at day 3 and 4, and day 9 and 10 after microdrive implant. The groups were compared at the two time-points and within the same groups at different time-points, using the Wilcoxon rank sum test. There were no significant differences. For control : chABC on day 3+4, p= 0.55, on day 9+10 p= 0.21. Firing rate (Hz) = spikes/second. Median= 0.6 (control day 3+4), 0.62 (chABC day 3+4), 0.52 (control day 9+10), 0.44 (chABC day 9+10). n (cells) = 20, 28, 13, 28.

Differences in activity (figure 3.5) were tested on a population level, but did not show any statistically significant differences ($p>0.2$ for all comparisons, Wilcoxon rank sum test), neither between the two groups, nor within the same group on different time-points. Cells appeared to be stable both with regards to physical and basic functional properties.

3.3.2 Neuronal activity after PNN degradation

As described in chapter 1.2.3, the PNN appears to be important in facilitation of the fast-spiking activity of inhibitory neurons. Inhibitory neurons play a large part in regulating and shaping the activity of pyramidal neurons, and so these excitatory cells could also be affected by any disruption of inhibitory cell activity. In order to investigate to what extent removal of the PNN affects the total activity of the neuronal network, cells were separated into pyramidal and inhibitory neuron populations. All the cells recorded between 3 and 21 days after microinjections/microdrive implant in chABC injected and control animals were compared on the basis of their firing rate,

when the animal was awake and presented with visual stimulation (controls n= 77, of which 17 were classified as inhibitory neurons, chABC n= 71, of which 10 were classified as inhibitory neurons).

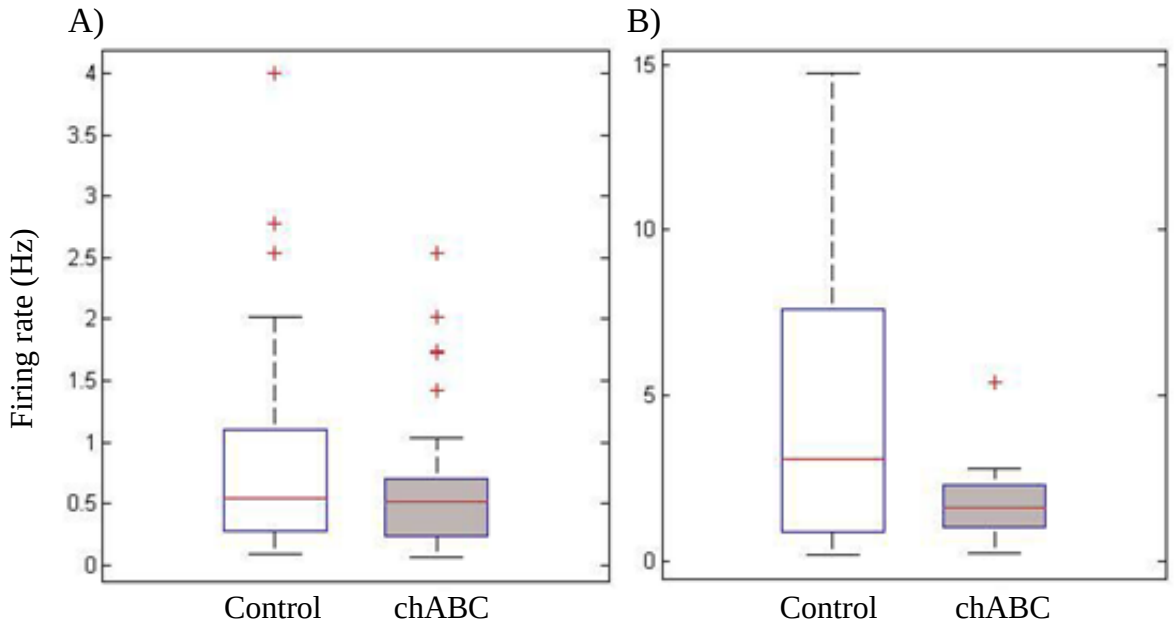

Figure 3.6: Firing rates of pyramidal cells and inhibitory neurons in control and chABC animals. As the PNN appears to be important for the maintenance of inhibitory neuron function, cell types were treated separately. Firing rate (Hz)=spikes/second **A)** Firing rates of pyramidal neurons, n=59 (control) n=61 (chABC). Wilcoxon rank sum test was applied. p= 0.08. Median= 0.55, SEM 0.09 (control), Median= 0.51, SEM= 0.06 (chABC). **B)** Firing rates of inhibitory neurons, n=17 (control) n=10 (chABC). Wilcoxon rank sum test was applied. p= 0.18. Median= 3.07, SEM= 1.12 (control), Median=1.61, SEM=0.45 (chABC). Despite the comparable low firing rates seen in the inhibitory neurons from the chABC sample, the data set was not significantly different from the control group.

Difference between groups with regards to pyramidal cells was not statistically significant (p=0.08, Wilcoxon rank sum test) (figure 3.6A), but the chABC treated group showed a slightly lower mean and median of firing rates. PNN degradation does not appear to influence the general activity of the pyramidal cells.

With regards to inhibitory neurons (figure 3.6B), the chABC groups was not significantly different from the controls (p=0.18, Wilcoxon rank sum test). Inhibitory neurons in chABC treated animals showed lower mean and median firing rates, as well as a much smaller variation within the population. This could be the result of the lack of PNNs to support the fast-spiking activity seen in the control group.

3.3.3 Tuning properties after PNN degradation

To investigate how degrading the PNN affects the functional properties of single cells, we investigated orientation selectivity of the cells in response to visual stimulation. This is an even further measure of how degrading the PNN affects the stability of the neuronal network. The tuning properties are developed during the CP, and are one of the qualities which seem to be "hard-wired" later in life, as described in chapter 1.1.1 and 1.1.2. The cell population used for this analysis was the same as that intended to be used to assess the effects of anesthesia. Inhibitory neurons have previously been shown to have little or no orientation selectivity (Niell and Stryker, 2008), but were included in the analysis nevertheless. The analysis was made based on recordings from anesthetized animals. They were presented with drifting gratings in 8 orientations (see figure 2.3), and the orientation preference was determined by calculating an orientation selectivity index (OSI), calculated as the ratio in firing rate : (firing $rate_{pref}$ – firing $rate_{orth}$)/(firing $rate_{pref}$ + firing $rate_{orth}$), where firing $rate_{orth}$ was the mean response of the two directions orthogonal to the preferred direction (Wang et al., 2010).

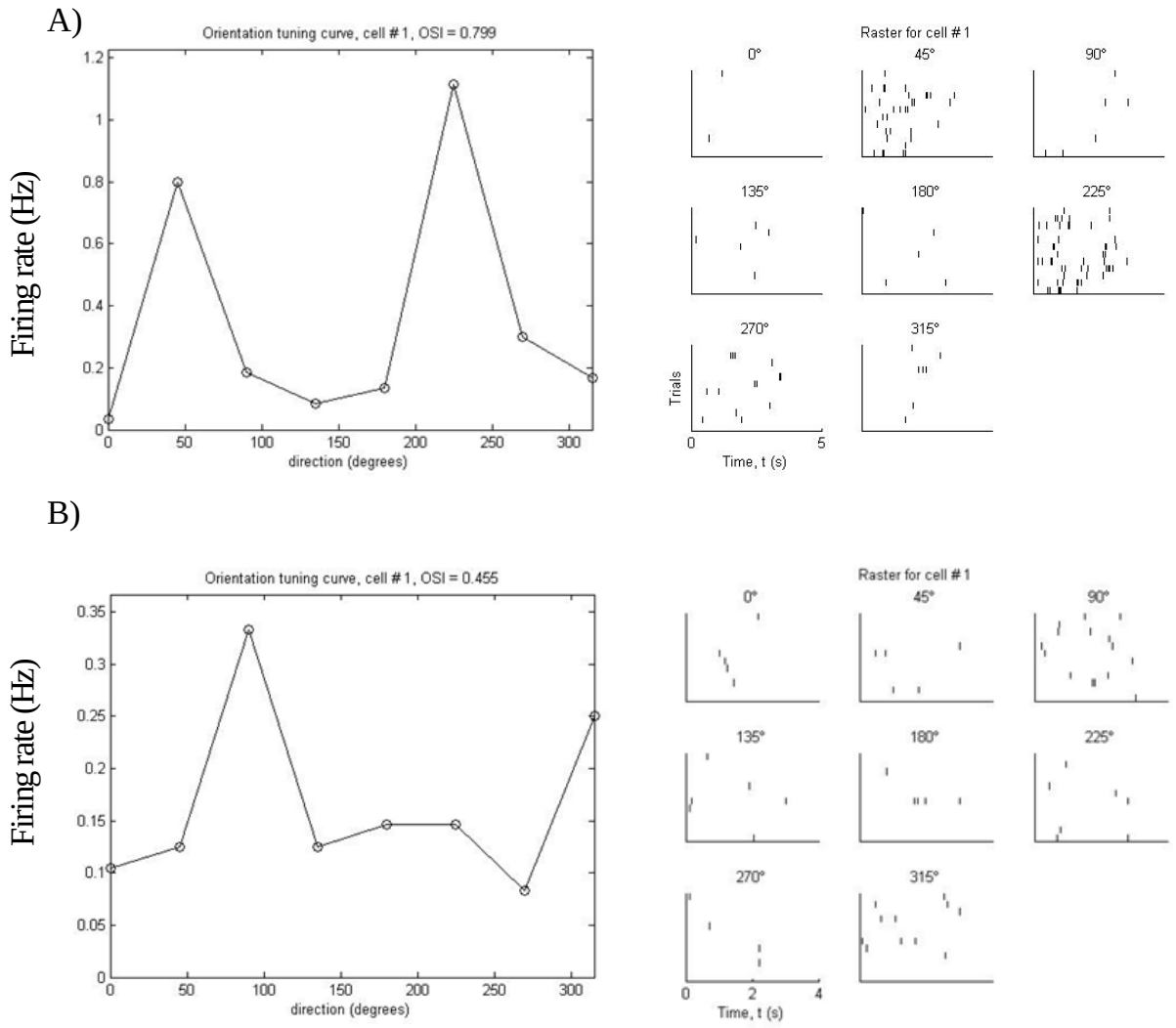

Figure 3.7: Examples of orientation tuning in V1 neurons in chABC injected and control animal. Visual stimuli were presented for three seconds, interleaved by a grey screen. Drifting gratings in 8 different orientations were presented in random order, 12 times each. Raster plots to the right show spikes in the different orientations presented; the y-axis shows time (s) and the y-axis indicates each of the 12 repetitions. The raster plots belong to the respective tuning curves shown to the left. Firing rate (Hz)=spikes/second. **A)** A cell in a chABC injected animal, selective for stimulation in 45° and 225° orientations. **B)** A cell in a control animal, selective for stimulation in 90° and 315° orientations.

Neurons from both chABC injected and control animals had receptive fields with sharp tuning curves (figure 3.7 A and B) and neurons which displayed little or no orientation selectivity. In addition, some neurons showed no apparent preference, but where the cell was strongly inhibited at one or more orientations (figure 3.8).

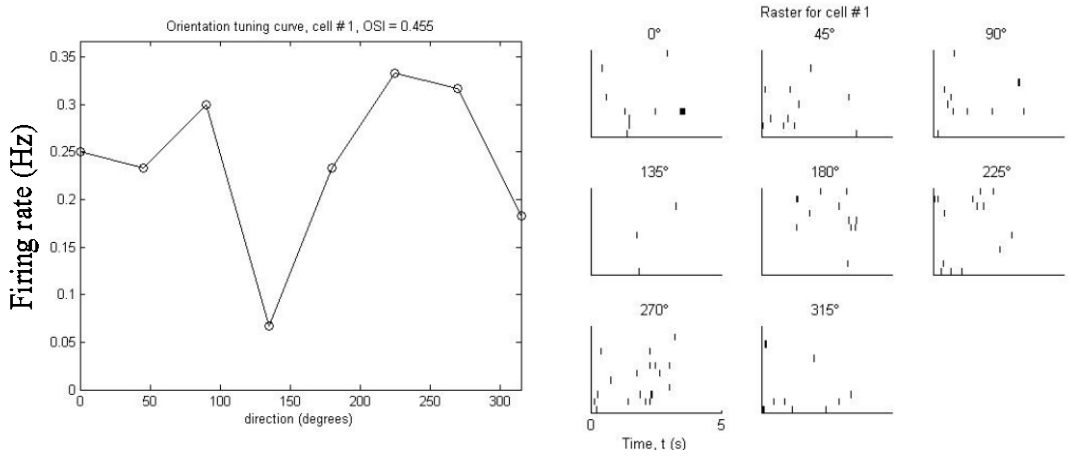

Figure 3.82: A cell in V1 with no apparent preference for any of the 8 orientations presented, which is inhibited at 135°. Raster plots to the right show spikes in the different orientations presented; the y-axis shows time (s) and the y-axis indicates each of the 12 repetitions.

In order to compare controls and chABC groups, a threshold of 0.3 in OSI was set: cells with OSIs lower than this were classified as not tuned for any specific orientation. Population sizes were 16 cells (control) and 22 cells (chABC), and it should be noted that apart from four cells, the data in the control population was based on recordings made in just one animal. The control group was initially larger, but because of a malfunction in the acquisition software synchronizing visual stimuli and the electrophysiological recordings, data from several recorded cells could not be included in the analysis.

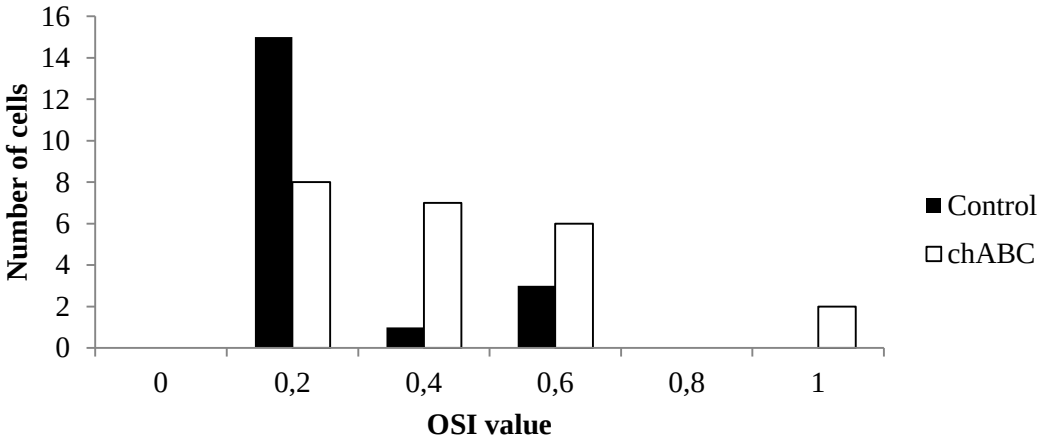

Figure 3.9: Histogram showing distribution of orientation selectivity index (OSI) in chABC injected and control animals. Population sizes were 16 cells (control) and 22 cells (chABC).

There was a significant difference when comparing OSIs between the chABC injected and control group ($p<0.01$, Wilcoxon rank sum test) but the control group in this analysis deviated from what was expected, likely because of the small population size. Only 17% of the 16 control cells had an OSI value above 0.3, where one would normally expect approximately 40% (Girman et al., 1999). Cells from chABC injected animals, however, showed this degree of tuning, where 41% of the 22 cells had an OSI value above 0.3. The tuning properties of cells in chABC injected animals were therefore, most likely, unaltered.

3.3.4 Effects on local field potential oscillations

The local field potential (LFP) oscillations are the combined output of the activity of all cells in an area. The synchronized activity of LFP oscillations has been related to several behaviors, and to the transfer of information between brain areas (see chapter 1.2.5 and 2.6.4). As described in chapter 1.1.4, the PV^+ cells are generators of gamma frequency oscillations (30-80 Hz) which usually restricts to local populations, while theta frequency oscillations (5-10 Hz) are spread across brain areas. Hence, to compare the control and chABC animals at these two frequency ranges could be a good measure as to how the PNNs contribute to the generation and maintenance of LFP oscillations.

In order to elucidate how the PNNs affect LFP oscillations, EEG recordings were compared on the basis of power spectrums and changes in LFP over time. We used theta and gamma peak values, a measure of which frequency within defined areas of theta and gamma frequency bands are most abundant, and wavelet analysis, to investigate whether there were any differences between chABC injected and control animals. In figure 3.10, results from such an analysis of an animal with bilateral chABC injections can be seen. As a pilot study, this was analyzed in recordings from one animal with bilateral chABC injections, one animal with chABC injected in one hemisphere, and a control animal.

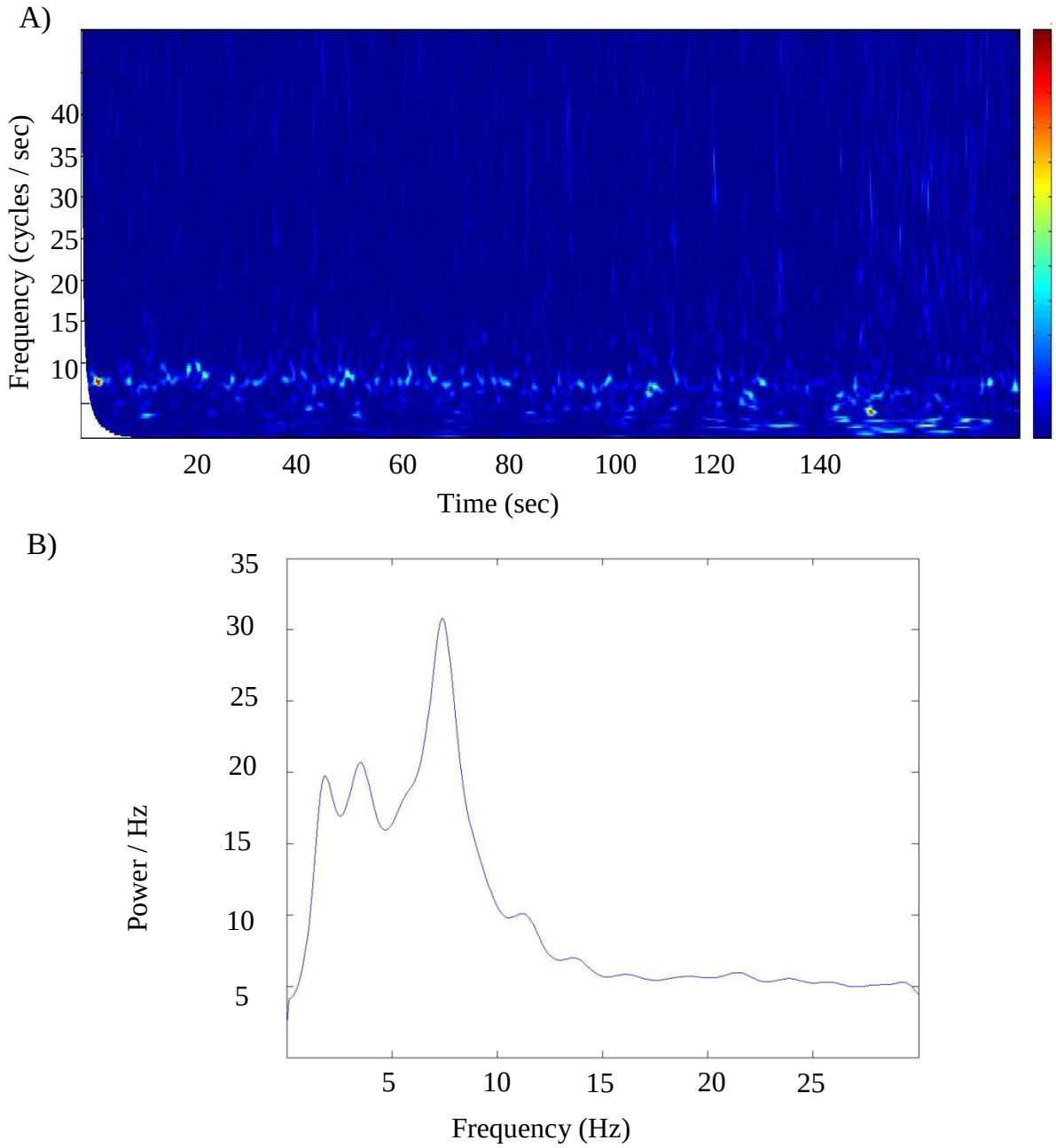

Figure 3.10: Recordings of local field potential (LFP) dominated by oscillations in the theta frequency band, from a chABC injected animal. **A**) Wavelet analysis shows the changes in LFP over time, and the color indicates power, or abundance of the different frequencies. Color coding on the right (dark blue= no activity in the given frequency, red=all the activity is in the given frequency). **B**) Power spectrum of the same recording as in A. The power spectrum shows the abundance of frequencies relative to each other, during one recording.

The groups were compared on the basis of power peaks within the theta and gamma frequency bands. Gamma frequency oscillations can be hard to detect in a power spectrum, but the wavelet figure shows bursts of gamma activity. The initial analysis did not indicate any differences between the groups (data not shown) and I did not pursue this further.

3.4 Effects of monocular deprivation

3.4.1 Ocular dominance plasticity after PNN degradation

The PNN has been suggested to be a major break for plasticity in adult animals, and its degradation has been shown to lead to increased plasticity (see chapter 1.2.3). To investigate the effects of PNN degradation on plasticity, four chABC injected and two control animals underwent MD for five days. Neurons were recorded before, during and after MD, and the visual modulation and OD preferences were determined. By comparing the responses of single neurons upon stimulation of each of the eyes, the OD index (ODI) was calculated as the difference in firing rate between responses to stimulation of contralateral and ipsilateral eye, divided by the sum; (firing $\text{rate}_{\text{contra}}$ − firing $\text{rate}_{\text{ipsi}}$) / (firing $\text{rate}_{\text{contra}}$ + firing $\text{rate}_{\text{ipsi}}$) (Wang et al., 2010). An ODI value between 0.05 and 1 indicated contralateral bias, and an ODI value between -0.05 and -1 indicated ipsilateral bias. ODI values between 0.05 and -0.05 indicated equal response to both eyes. The classification was made on cells in the hemisphere contralateral to the deprived eye.

A)

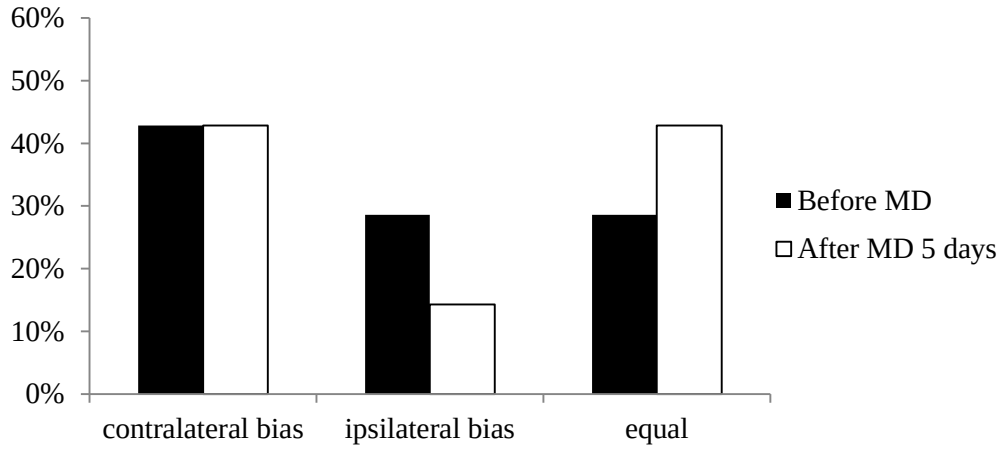

B)

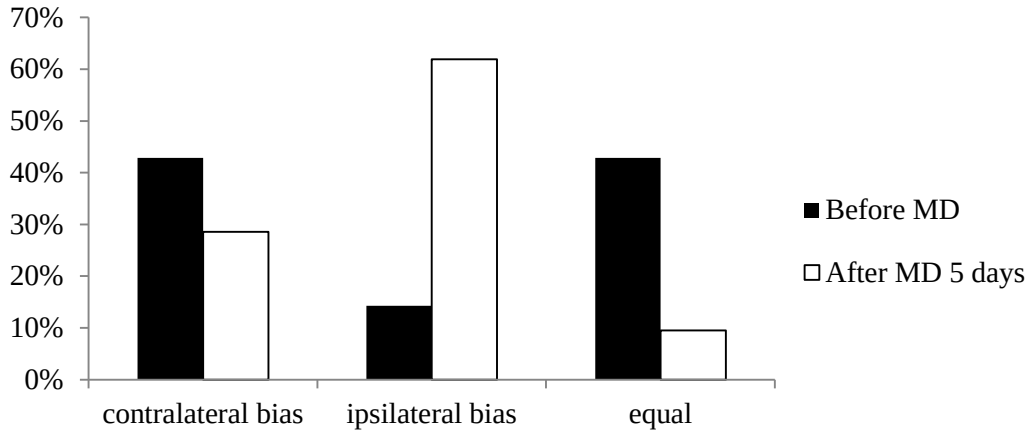

Figure 3.11: Cortical activation bias before and after 5 days of MD in chABC-injected and control animals. The classification was based on single cells' responses to stimulation of each of the eyes. An ODI was calculated for each cell by measurement of firing rate: (contra – ipsi) / (contra + ipsi) – an ODI value between 0.05 and 1 indicated contralateral bias, an ODI value between -0.05 and -1 indicated ipsilateral bias. ODI values between 0.05 and -0.05 indicated equal response to either eye. **A)** Cortical activation in control animals before and after MD. A small but significant change was seen. n=7 (before MD), n= 7 (after MD). The mean ODI changed from -0.0003 to 0.009, $p<0.01$ (Wilcoxon signed rank test). **B)** Cortical activation in chABC injected animals before and after 5 days of MD shows the opposite pattern of the control. A shift in activation towards the non-deprived eye has occurred, with the mean ODI of the population shifted from 0.05 to -0.09, $p<0.001$ (Wilcoxon signed rank test). n= 7 (before MD), n= 21 (after MD).

In control animals (n = 7 cells before and after MD) (figure 3.11A) there was a significant change in ODI values ($p<0.01$, Wilcoxon signed rank test), but the mean ODI values before and after MD were very similar (-0.0003 before MD, 0.009 after MD). The significant result could be due to the small population size. Others have

previously reported little of no effect of MD for five days in adult, untreated animals (Sato and Stryker, 2008).

In chABC injected animals, however, there was a large effect of MD on OD distribution (n (before MD= 7 cells, after MD=21 cells) (figure 3.11B), and a significant change in ODI values ($p<0.001$, Wilcoxon signed rank test). The mean ODI value shifted from 0.05 before MD to -0.09 after MD, indicating that the MD period had produced a shift in OD. Before MD, 14% (3/7) of cells had ODI values favoring the ipsilateral eye; in contrast, after MD, 62% (13/21) of cells had ODI values which favored the non-deprived, ipsilateral eye.

3.4.2 Effects of sensory deprivation on single cells

In order to understand the basis of the functional changes seen after MD in chABC injected animals, I investigated activity in single cells before and during the MD period. The same populations of pyramidal cells were recorded from repeatedly across days, and their activity between days was compared.

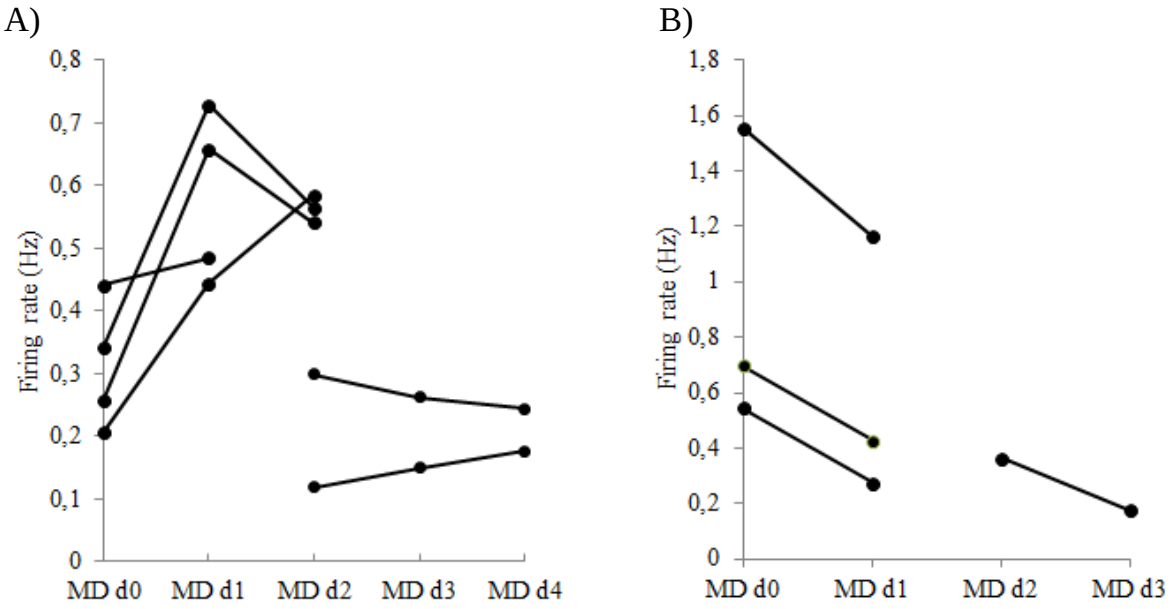

Figure 3.12: Changes in activity in single neurons during MD. The same neurons were recorded over 2-3 days before and during the 5-day MD period in chABC-injected animals: firing rates are shown as individual data points. Each point on the same line represents the same cell at different points in time. **A)** Cells on the ipsilateral side of the deprived eye showed increased firing rates after 1-2 days of MD, after which this stabilized (mean increase from MD day0 to MD day 1= 99.5%). **B)** Cells on the contralateral side showed a large reduction in firing rate; this reduction continued throughout the period (mean decrease from MD day0 to MD day 1= 38%).

The activity of the neurons in the ipsilateral side showed a large increase in activity (mean increase MD day 0-MD day 1 = 99.5%) from the start of MD and one to two days, before it stabilized (figure 3.12A).

Neurons on the contralateral side showed reduced activity; this tendency continued throughout the MD period (figure 3.12B) (mean decrease MD day-MD day1 = 38%, mean decrease MD day 2-MD day3 = 52%).

3.5 Effects of anesthesia

3.5.1 Effects on neuronal activity

The use of anesthesia has severe effects on cortical processing, but the effects on single neurons in V1 are not clear (see chapter 1.4.1). To assess the effects of anesthesia on processing in V1, we recorded the responses of 38 cells in chABC injected and control animals, and compared their activity and tuning properties when the animal was awake and anesthetized. We monitored the activity in cells when the animals were awake, and the same cells 10-15 minutes into anesthesia. There were no differences between the chABC treated and control animals ($p=0.63$, Wilcoxon rank sum test), so data from these groups were pooled for the anesthesia analysis. The majority of cells (24/38, or 63%) showed reduced activity in the anesthetized compared to awake state; of these, one third (8 cells) went completely silent. Twenty nine percent of cells (11/38) showed an increase in activity in anesthesia; these included all the inhibitory neurons in the population, although pyramidal cells also showed increase in activity.

In order to quantify the variability in response to anesthesia observed, we calculated the ratio in firing rate for the same cell in awake vs. anesthesia. The calculation was made by $(\text{firing rate}_{\text{anesthesia}} - \text{firing rate}_{\text{awake}}) / (\text{firing rate}_{\text{anesthesia}} + \text{firing rate}_{\text{awake}})$, where a value between 0 and 1 indicates an increase in activity and a value between 0 and -1 indicates a decrease (figure 3.13).

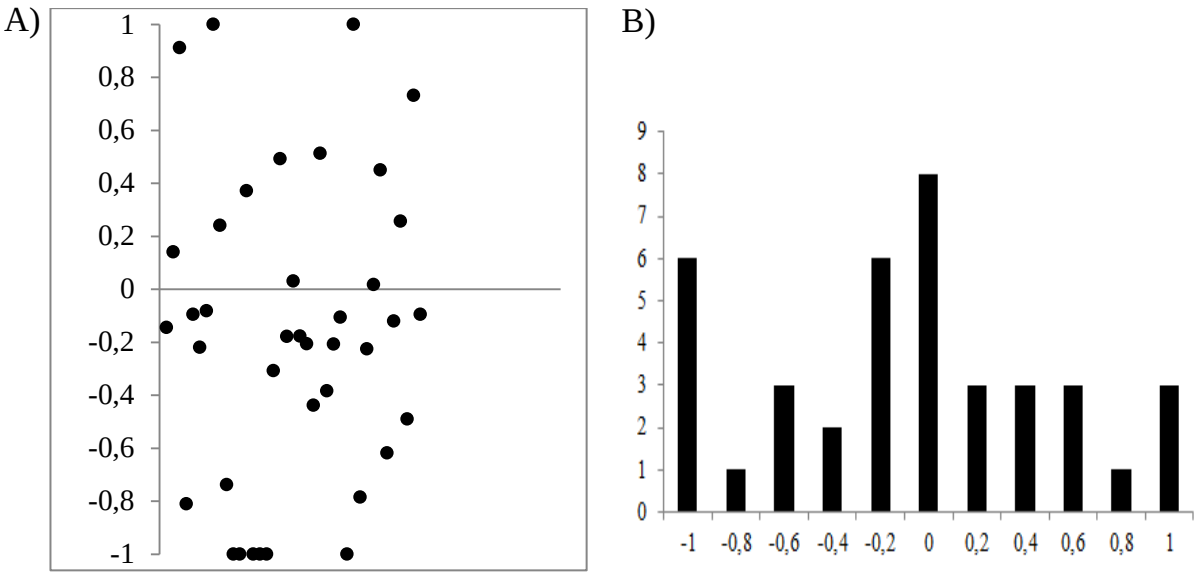

Figure 3.13: The ratio between firing rate in the awake and anesthetized state shows large variation in regards to how cells respond to anesthesia. The ratio was calculated by (firing rate $_{anesthesia}$ - firing rate $_{awake}$) / (firing rate $_{anesthesia}$ + firing rate $_{awake}$). Cells with an increase in activity are between 0 and 1, while cells with a decrease in activity are between 0 and -1. The data are skewed towards the negative values in the histogram (**B**), indicating that the majority of the neurons reduced their firing rate when the animal was anesthetized. n= 38, and includes data from both chABC injected and control animals.

The large variation in activity was observed in the population; it was also evident between neurons recorded simultaneously from the same anatomical position (from the same tetrode) (figure 3.14). Neurons recorded on the same tetrode showed highly different outcomes, where some showed a dramatic increase in activity, while others showed a dramatic reduction in activity.

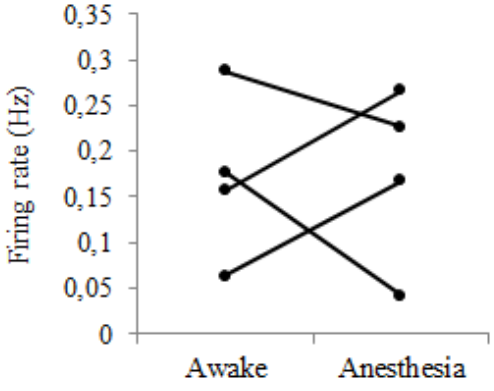

Figure 3.14: Neighboring neurons may respond differently to anesthesia. The four cells were recorded simultaneously on the same tetrode in the awake and anesthetized state, and responded very differently (in firing rate, Hz) to anesthesia.

3.5.2 Orientation selectivity in awake and anesthetized animals

We investigated whether it was possible to use recordings done in awake, freely behaving animals to assess orientation selectivity, and compared these to recordings of the very same neurons in the anesthetized state. The classification was again made by comparing OSI values, and the threshold set at 0.3 as before. Because tuning properties between chABC injected and controls were different, the groups were treated separately. Initially, there did not appear to be any major difference; of the cells in the chABC group, 38% of cells were above the threshold in awake, with 41% in anesthesia. For controls, 13% were above threshold in awake, with 17% above in anesthesia. However, when comparing several recordings from the same session, cell from anesthesia were stable and showed the same tuning in consecutive recordings, while cells from awake were highly variable; less than 10% of cells showed the same orientation tuning in two or more recordings, and, indeed, the same tuning in awake as in anesthesia. Furthermore, just as with firing rates in single cells, the changes between awake and anesthesia were highly variable, as some cells showed stable tuning while others were completely different in the two states. Shown below (figure 3.15 A and B) are tuning curves from two neurons in a chABC injected animals. The neurons were recorded from the same tetrode in awake and anesthesia; one has the same, strong tuning in both states (OSI >0.8), while the other has no apparent preference in awake, but a fairly strong tuning in anesthesia (OSI = 0.12 and 0.42).

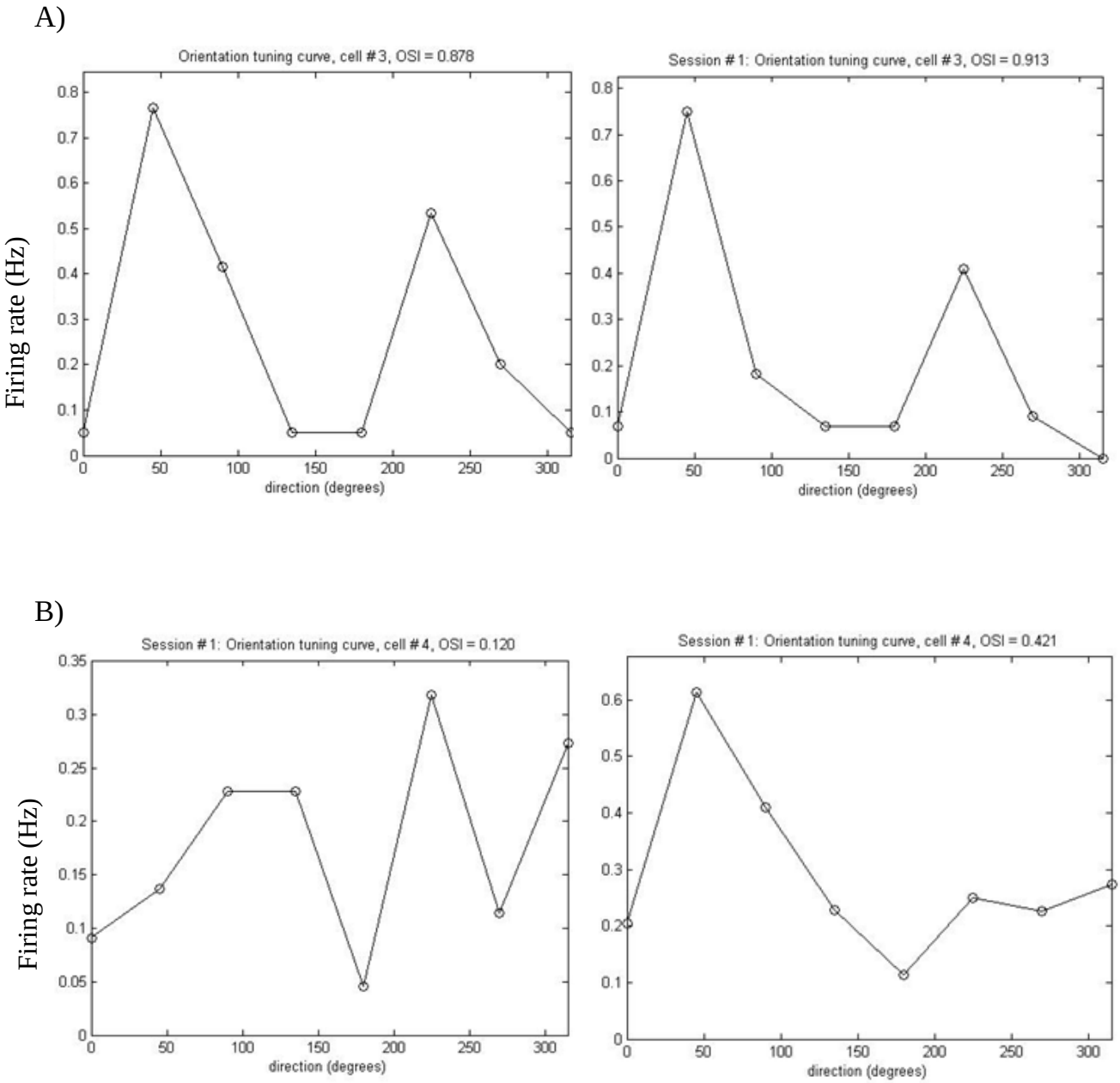

Figure 3.153: Tuning curves of the same neurons in the awake and anesthetized state. Two neurons recorded from the very same tetrode show very different orientation selectivity in the two states. **A)** Cell 1 has a strong orientation selectivity in both awake (left) and anesthesia (right), with an OSI >0.8 in both states. **B)** Cell 2 has no apparent orientation selectivity in awake (OSI = 0.12), but shows s fairly strong preference for 45° stimuli in anesthesia (OSI = 0.42).

These observations raise some interesting questions regarding the effects of anesthesia that will be discussed. These effects are in line with preliminary findings by another member of the Hafting-Fyhn lab, Ida Aasebø, who is performing a comprehensive study on the effects on anesthesia on visual processing.

4 Discussion

This work shows that enzymatic degradation of PNNs in the visual cortex leads to reduced activity of inhibitory neurons, but no other apparent changes to the response properties of neurons in the visual cortex. Furthermore, removal of the PNNs opened up a period of heightened plasticity in the adult rat. The present study is the first to perform longitudinal recordings of ensembles of well isolated neurons in V1 during sensory deprivation in a period of heightened plasticity. I found that cortical neurons ipsilateral to the deprived eye showed a potentiation of activity within the first 24 hours, while neurons contralateral to the deprived eye showed reduced activity throughout the period of sensory deprivation. These results stand in contrast to previous studies, as will be discussed below.

My study provides the first quantitative description of the regeneration of PNNs after enzymatic degradation. The gradual regeneration should be of interest both with respect to biochemical and clinical research and for future functional studies, as it provides a time-frame for the turnover of matrix molecules in the PNN structure. Additionally, I show that the use of anesthetics has both profound, and highly variable, effects on neuronal populations in the cortex. The differences in neural responses between the awake and anesthetized state affects implications of results on information processing from experiments conducted under anesthesia.

4.1 Methodological considerations

There are several advantages in using multi-electrode recording equipment, such as tetrodes, when investigating neuronal processing in the brain. Unlike single-electrode equipment (e.g. tungsten electrodes), multi-electrode recordings give insight into activity of whole neuronal populations and the interplay within these, as well as the activity of single cells (Buzsaki, 2004). Additionally, the use of multi-electrode recordings provide a means to acquire a large dataset from chronic experiments. With tetrodes, one can simultaneously record from many cells, and when used chronically, their depth can be adjusted through different cell layers over the course of the experiment. In contrast, single electrode recordings require the insertion of the

electrode at many locations in the brain area of interest in order to acquire data sets of similar magnitude. Hence, these experiments are usually performed in acute preparations, where the animal is anesthetized during the experiment and sacrificed at the end of the recordings. This gives a certain degree of bias towards recording cells with high activity, whereas multi-electrodes provide a more unbiased sample of the population.

However, chronic experiments with multi-electrodes are technically demanding experiments, and the risk of damaging the cortex upon implantation is significant; measurements of neuronal activity in the superficial cell layers often begin only 200 µm below the surface of the dura mater. Furthermore, the offline spike-sorting is done manually and may be subject to some degree of bias. As an attempt to avoid this, I completed all spike-sorting in this study before any analyses of visual properties were performed. The spike-sorting is time consuming and very challenging, illustrated by the large amount of data currently left out of the analysis in this study.

Only a handful of studies of visual processing in rodents have been performed using tetrodes (Ji and Wilson, 2006; Szuts et al., 2011; Arnold et al., 2013). To the best of my knowledge, this is the first study to use chronically implanted tetrodes to measure neuronal activity during MD, and the very first to combine the use of tetrodes with microinjections in the visual cortex.

We chose to use glass pipettes for the injections. While the most common method for microinjections is to do one large injection, using for instance a Hamilton syringe, this may cause tissue damage which could ruin the electrophysiological recordings. The use of thin glass pipettes, on the other hand, leaves very little damage to the tissue which we were not able to detect later on the histology sections (figure 3.1). Several small injections secured good coverage, spanning almost the entire visual cortex. Pizzorusso *et al.* (2002), and others after them, performed injections of chABC three days in a row. However, I determined early in this study that one set of injections was sufficient to degrade the PNN completely (figure 3.2A). In addition to being time saving, this protocol reduced the risk of infections, damage to the cortex and stress to the animals.

Immunohistochemical labeling of PNNs was done by two different procedures. Initially, sections were fixated to a glass slide before staining, but this produced highly variable results, where only approximately 25% of the sections were stained and the whole PNN structure could rarely be seen. Instead, I then attempted to stain sections while they were free-floating in solution. The latter produced consistent results, with highly improved tissue penetration of the antibodies.

There is a rather large difference in quality of the images presented in the Results chapter, because the images were acquired using two different microscope setups, one with low resolution (3 megapixels) and one with very high resolution (63 megapixels). The low-resolution setup was used to photograph all WFA stained sections from brains where the animal had been used for electrophysiology. I did not know which section contained the tetrode track prior to Nissl staining; with the low-resolution setup 25 sections could be photographed in approximately 30 minutes. In contrast, photographing and stitching of a single section with the high-resolution setup took approximately 15 minutes. Nissl staining sections had to be performed quickly after the sections had dried on the slide, in order to achieve high quality. However, the low-resolution images was of sufficient quality for the greyscale measurements to be performed, as the PNNs were clearly seen around cell bodies and dendrites and the measurement is dependent on color intensity. The issue of starting the Nissl staining shortly after PNN labeling was the only challenge when counterstaining PNNs and Nissl bodies. Others have reported several problems when Nissl staining after immunohistochemical labeling (Kádár et al., 2009), but the protocol I have developed here appears to be very sensitive to the tissue (figure 3.1A).

4.2 The impact on cortical neurons of microinjections and tetrode implant

As discussed in chapter 1.2.3, glia cells will respond to damage in the CNS. In order to ensure that the microinjections and tetrode implant did not cause a lot of damage to cortical neurons, sections were stained for Nissl bodies and glia cells (figure 3.1). While the damage caused by the tetrodes did vary to some extent, the cell layers were generally intact. Recording positions of the tetrodes were verified with a fairly high

accuracy (±100 µm). With regards to the glial response, I did not detect any up-regulation of glia cells near the tetrode track, nor around the injection sites. This indicates that the tissue remained relatively intact throughout the experiments, and that neither of the interventions caused visible damage. Similarly, the actual degradation of PNNs did not appear to produce a glial response.

4.3 PNN regeneration

To the best of my knowledge, Brückner *et al.* (1998) is the only study investigating the regeneration of PNNs after enzymatic degradation. In their study, animals were injected with chABC and sacrificed at different time points: after 1 day, 1, 2, 3, 4, 8 and 12 weeks, and 5 months. However, in the paper, they only show histology from 1 day, 4 weeks and 5 months after chABC injections, and there were no quantitative measurements. In order to establish a temporal window for functional studies, I injected chABC and sacrificed animals at seven time-points from 3-60 days after injections (figure 3.2). The sections were stained with WFA, and the ratio between the injected area and a control area measured using greyscale measurement. Three days after injection, the PNN was completely degraded, and thus the other measurements were normalized relative to this ratio. The results shows that the regeneration is gradual, with the largest increase in labeling happening from day 10-21 (figure 3.3B). The epitope for WFA has not yet been determined, and it remains elusive at what time-point the epitope assembles into the PNN. However, staining with WFA has been the standard for labeling PNNs for more than 15 years, and is considered rather robust. Furthermore, it is not entirely clear how long the enzyme remains active *in vivo*. My results show that during the first 10 days, less than 5 % of the PNN is regenerated. Hence, I performed the MD studies within the first 10 days in order to optimize conditions for plasticity. The other electrophysiological studies were performed within 21 days of enzyme injection, but there were no detectable changes in activity during this period. Most neurons were, however, recorded three and 12 days after surgery. While tissue and staining quality varied to some extent, the histological analysis provided here presents a good framework for future studies of PNN function, giving the first quantitative measure of the extent of regeneration of the PNN.

4.4 The effects of PNN degradation on cortical processing

The measurements of activity in a large population over time following chABC injections, such as performed in this thesis, had not been done before. I did not observe any changes with regards to activity and stability of pyramidal cells after enzymatic degradation of the PNN (figure 3.4., 3.5 and 3.6A). Considering the prospective use of chABC as a therapeutic agent for rehabilitation after both spinal cord injury and stroke, these results are highly relevant and encouraging.

There was a strong tendency towards a large decrease in activity of inhibitory neurons in the population of neurons from chABC injected cortices (figure 3.6B). While no differences were seen in waveform, firing rates were strongly reduced compared to controls. This result was not significant, but that is likely due to the rather small population size of only 27 cells. Furthermore, we have only used the Wilcoxon rank sum test, while other statistical analyses, such as a generalized linear model could have yielded a different outcome. One would expect the data to normally distributed, but because the data set is small, this was not the case. Assumed that this was a normally distributed population, the Student's t-test gives a significant difference between the chABC and control group ($p= 0.04$).
The reduction in activity supports what others have found with regards to the interplay between PV^+ neurons and the PNN. It has been shown that the removal of the PNN distorts calcium transients in the PV^+ cells, and that the large reduction in Otx2 capture disrupts normal PV^+ cell function (Hrabetova et al., 2009; Beurdeley et al., 2012).

There was a significant difference between groups in orientation tuning, but this was again most likely skewed by small population sizes. The data in the control group was to a large extent based on data from one animal; in addition to being a small population the position of the tetrodes in this one animal could be the reason for the low percentage of cells which showed tuning. When comparing tuning properties of chABC injected animals (figure 3.9) to that of other studies (Girman et al., 1999; Niell and Stryker, 2008), the tuning properties of the chABC injected group was not different. This supports earlier findings by Pizzorusso *et al.* (2002), who showed that PNN degradation did not affect orientation selectivity or visual acuity, through single-

electrode recordings. However, I have only investigated orientation selectivity. Direction selectivity has been reported to be NMDA-receptor dependent, which would indicate that this is a trait more susceptible to change in an environment of heightened plasticity (Mehta and Wilson, 2000). Additionally, recent reports suggest that by reducing inhibition, sizes of receptive fields in V1 increase (Harauzov et al., 2010). Such analyses were beyond the scope of this project, but the dataset could be used to investigate such properties later.

We did not see any changes in oscillations in the gamma frequency band. This was surprising, as the PV^+ cells are the local generators of gamma frequency oscillations (see chapter 1.1.4), and with the decrease in inhibitory neuron activity seen, including PV^+ cell activity, we expected to see some difference. Neither the occurrence of gamma oscillations, nor the frequency bands these were in, was different from controls. This could be due to the equipment used. While tetrodes have been used extensively to record LFP in other areas of the brain, e.g. the hippocampus and entorhinal cortex, their ability to detect changes within small populations is somewhat unclear. The differences in the cortex could be very local, while in the hippocampus, the slow oscillations spread through large populations.

The connection between PV^+ cells and PNNs in relation to LFP oscillations is interesting in relation to several neurological disorders. In schizophrenia, a reduction in GABAergic transmission in PV^+ cells causes a reduction in gamma frequency oscillations (Lewis et al., 2005). This is known to impair working memory, a symptom seen in many schizophrenia patients (Wilson et al., 1994; Lewis et al., 2005), and post-mortem investigations indicate that the PNN is abnormal in structure and composition in schizophrenia patients (Pantazopoulos H, 2010; Berretta, 2012). In the development of epilepsy there is an abnormally high level of synaptogenesis and a failure in the PV^+ cells' ability to synchronize local populations, both of which might indicate a role for PNNs (Schwaller et al., 2004; McRae and Porter, 2012). Conversely, the PNNs appear to have a neuroprotective effect against oxidative stress, as in the case of Alzheimer's disease, and in early development of schizophrenia (Morawski et al., 2012; Suttkus et

al., 2012; Cabungcal et al., 2013). Local field potential oscillations after PNN degradation should be investigated further in the current data set.

4.5 Effects of monocular deprivation in chABC injected animals

Monocular deprivation following PNN degradation caused a shift in OD properties in chABC injected animals (figure 3.11), as others have shown before (Pizzorusso et al., 2002; Pizzorusso et al., 2006). In this study, however, the experiments were performed chronically, meaning that OD distribution was determined in the same animals before and after MD, rather than in two groups of animals (one sensory deprived and one untreated). This provides a much more solid ground of evidence. Furthermore, it gives the unique opportunity to record from the same cells at several time-points during the MD period; these data are the first of their kind. Only one earlier study has attempted to measure neuronal activity during MD (Frenkel and Bear, 2004), but through the use of visually evoked potentials (VEPs) in critical period aged mice. This technique is a kind of LFP measurement, where one can measure population activity in response to stimuli but not distinguish single cells. My recordings from single cells somewhat conflict with these results; Frenkel *et al.* (2004) reported that in CP mice, the contralateral reduction in activity is immediate, while the ipsilateral potentiation is delayed until day 5 of MD. My study, however, indicates that the potentiation in activity ipsilateral to the deprived eye happens within the first 24 to 48 hours, after which the activity stabilizes (figure 3.12). While the populations are small, these tendencies are consistent throughout all the recordings.
Most previous studies on OD properties in rodents have been performed during the CP. However, it has also been shown in adult mice that MD for 8 days or more produces a significant shift in OD (Sato and Stryker, 2008). Hence, to avoid false positives the MD period in my study was 5 days to avoid effects in control animals. Pizzorusso *et al.* (2002, 2006) did MD for 8 and 15 days which may have activated plasticity responses not associated with the removal of PNNs.

The elevated levels of plasticity that follows PNN degradation can be viewed both as a result of functional and structural changes, although the precise mechanisms are not clear. The PNN has been shown to be an important regulator of synapse formation and

receptor density with synapses (Pyka et al., 2011), and axonal growth has been shown to be inhibited by CSPGs, although the latter seems to depend on the sulfation pattern (Snow et al., 1994; Lin et al., 2011). Together, this supports the idea that the PNN functions as a break on synaptic reorganization and synaptogenesis, both through functional interactions and as a structural barrier.

The central role of inhibition during the CP is well established. The interplay between PV^+ inhibitory neurons and the PNN seems to be the most important factor in the regulation of plasticity, a hypothesis supported by the reduction of inhibitory neuron activity observed in this study. Non-specific reduction of inhibitory activity through infusion of a GABA antagonist has been shown to lead to increased plasticity (Harauzov et al., 2010). Interestingly, this also caused a reduction in the labeling of PNNs, suggesting that the regulation of PV^+ activity by the PNN might in fact be bi-directional, and that the normal turnover of the PNN is quite rapid. In mouse models with reduced GABAergic transmission, the animals do not undergo a CP unless pharmacologically induced (Hensch et al., 1998; Fagiolini and Hensch, 2000). It would be very interesting to investigate the PNNs of such animal models, to further investigate the role of PV^+ cells and PNNs and how they regulate each other.

The reduction in activity seen after PNN degradation could, in part, be the result of a reduction in Otx2 uptake, which is usually facilitated by the PNN. It has been suggested that, much like for the total level of inhibition, the PV^+ cells require an amount of Otx2 uptake within a defined window to allow for plasticity; when the levels exceed the upper threshold going into adulthood, plasticity is abolished (Sugiyama et al., 2008). To what extent this contributed in this study has not been accounted for, and considering the short time-span of the study, it might be more likely that the loss of a favorable ionic milieu for fast-spiking activity, as a result of degradation of the PNN, was the more important factor.

4.6 Effects of anesthesia

While anesthesia has been widely used to study visual processing for more than 50 years, very few studies have addressed how general anesthetics affect processing compared to awake animals (Greenberg et al., 2008; Niell and Stryker, 2010). The data

on the effects of anesthetics are part of a comprehensive study on the effects of anesthesia, conducted by Ida Aasebø in the Hafting-Fyhn research group. I found that the general anesthetic Midazolam has profound and highly variable effects on cortical neurons, both with respect to firing rate and orientation selectivity (figure 3.13 and 3.15). Of particular interest are the neurons recorded on the same tetrode, which responded differently to anesthesia (figure 3.14 and 3.15). These are anatomically closely positioned neurons which showed differences both in activity and tuning properties between the two states. This variation indicates fundamental differences in information processing in the awake and anesthetized states. If change in visual tuning curves were caused by a change in the visual field due to movements of the animals while awake, one would expect similar changes in tuning curves. The large variation in responses seen, however, indicates more fundamental differences in information processing on the level of the neural network. This may indicate multimodal sensory input, and individual effects of attentional control on the single cell level. The latter would correspond well to what was found by Niell and Stryker (2011) when comparing visual responses in different behavioral states, e.g. while sleeping and running. Altogether, the results presented in this study suggest that while anesthesia may be necessary to investigate specific tuning properties of neurons, the large differences in response to anesthetics by should be taken into consideration when performing such experiments.

4.7 Future perspectives

As some of the experiments performed in this study yielded inconclusive results, they should be repeated in order to increase the population sizes. This could further clarify the role of PNNs in cortical processing. Furthermore, the data set contains more data than was included in the analysis; when analyzed these data may support the current findings. With regards to the experiments discussed above, one should:

- Increase populations of inhibitory neurons, preferably enough to be able to segregate fast-spiking and others into two separate populations.

- Increase populations sizes of cells recorded during the first days of MD in chABC injected animals, especially since the results differ from earlier work (Frenkel and Bear, 2004). With a larger population it would also be possible to determine how fast the functional changes of OD happens; by comparing spontaneous firing rates to firing rates when visually stimulated, one could determine whether the increase in activity is the result of a general stress to the system, or an early indication of a functional change.

- Investigate further the effects of PNN degradation on LFP oscillations. Several recent studies have linked PV^+ cell malfunction to schizophrenia and epilepsy, and to determine the impact of PNNs on LFP oscillations would be of significant value in this regard.

Identifying the role of PNNs in regulation of PV^+ cell activity should be pursued, as this seems to be a key feature in regulation of critical period plasticity, adult plasticity, and important in the pathophysiology of several neurological disorders. With the emergence of new methods, such as the combination of two-photon microscopy and genetically modified animals, one could follow the same cells and monitor structural changes over time. Conditional knock-outs of the genes coding for the different elements of the PNN could provide valuable information, both with regards to understanding the physiology of the PV^+ cells and the PNN, and in relation to pathophysiology.

4.8 Conclusions

Based on the results from this study, I conclude that:

-After enzymatic degradation, the PNN reassembles over 60-100 days, and studies of the effects of PNN removal on cortical function should be performed within 14 days after chABC injection.
-Enzymatic degradation of the PNN does not alter basic tuning properties of pyramidal cells in the visual cortex.
-Enzymatic degradation of the PNN leads to a reduction in the activity of inhibitory neurons, and this reduction may be responsible for the increased plasticity seen in these animals.
-Monocular deprivation in chABC injected animals causes a shift in OD within days, and the earliest indications of the functional changes can be seen as early as one day into the MD period.
-General anesthetics have profound and highly variable effects on neuronal populations, both with regards to activity and to tuning properties. This should be taken into account when performing experiments on anesthetized animals.

References

Antonini, A. and Stryker, M. P. (1996). Plasticity of geniculocortical afferents following brief or prolonged monocular occlusion in the cat. *Journal of Comparative Neurology* 369, 64-82.

Arnold, M. M., Szczepanski, J., Montejo, N., Amigo, J. M., Wajnryb, E. and Sanchez-Vives, M. V. (2013). Information content in cortical spike trains during brain state transitions. *Journal of Sleep Research* 22, 13-21.

Asher, R. A., Scheibe, R. J., Keiser, H. D. and Bignami, A. (1995). On the existence of a cartilage-like proteoglycan and link proteins in the central nervous system. *GLIA* 13, 294-308.

Bach-y-Rita, P. and W. Kercel, S. (2003). Sensory substitution and the human–machine interface. *Trends in Cognitive Sciences* 7, 541-546.

Barritt, A. W., Davies, M., Marchand, F., Hartley, R., Grist, J., Yip, P., McMahon, S. B. and Bradbury, E. J. (2006). Chondroitinase ABC promotes sprouting of intact and injured spinal systems after spinal cord injury. *J Neurosci* 26, 10856-10867.

Berretta, S. (2012). Extracellular matrix abnormalities in schizophrenia. *Neuropharmacology* 62, 1584-1597.

Beurdeley, M., Spatazza, J., Lee, H. H., Sugiyama, S., Bernard, C., Di Nardo, A. A., Hensch, T. K. and Prochiantz, A. (2012). Otx2 binding to perineuronal nets persistently regulates plasticity in the mature visual cortex. *Journal of Neuroscience* 32, 9429-9437.

Blake, D. T. and Merzenich, M. M. (2002). Changes of AI Receptive Fields With Sound Density. *Journal of Neurophysiology* 88, 3409-3420.

Bliss, T. V. P. and Lomo, T. (1973). Long lasting potentiation of synaptic transmission in the dentate area of the anaesthetized rabbit following stimulation of the perforant path. *Journal of Physiology* 232, 331-356.

Bozdagi, O., Nagy, V., Kwei, K. T. and Huntley, G. W. (2007). In vivo roles for matrix metalloproteinase-9 in mature hippocampal synaptic physiology and plasticity. *Journal of Neurophysiol* 98, 334-344.

Bradbury, E. J., Moon, L. D. F., Popat, R. J., King, V. R., Bennett, G. S., Patel, P. N., Fawcett, J. W. and McMahon, S. B. (2002). Chondroitinase ABC promotes functional recovery after spinal cord injury. *Nature* 416, 636-640.

Brainard, D. H. (1997). The Psychophysics Toolbox. *Spat Vis* 10, 433-436.

Brauer, K., Hartig, W., Bigl, V. and Bruckner, G. (1993). Distribution of parvalbumin-containing neurons and lectin-binding perineuronal nets in the rat basal forebrain. *Brain Research* 631, 167-170.

Brückner, G., Bringmann, A., Härtig, W., Köppe, G., Delpech, B. and Brauer, K. (1998). Acute and long-lasting changes in extracellular-matrix chondroitin-sulphate proteoglycans induced by injection of chondroitinase ABC in the adult rat brain. *Experimental Brain Research* 121, 300-310.

Bush, T. G., Puvanachandra, N., Horner, C. H., Polito, A., Ostenfeld, T., Svendsen, C. N., Mucke, L., Johnson, M. H. and Sofroniew, M. V. (1999). Leukocyte infiltration, neuronal degeneration, and neurite outgrowth after ablation of scar-forming, reactive astrocytes in adult transgenic mice. *Neuron* 23, 297-308.

Buzás, P., Eysel, U. T., Adorján, P. and Kisvárday, Z. F. (2001). Axonal topography of cortical basket cells in relation to orientation, direction, and ocular dominance maps. *The Journal of Comparative Neurology* 437, 259-285.

Buzsaki, G. (2004). Large-scale recording of neuronal ensembles. *Nature Neuroscience* 7, 446-451.

Cabungcal, J.-H., Steullet, P., Morishita, H., Kraftsik, R., Cuenod, M., Hensch, T. K. and Do, K. Q. (2013). Perineuronal nets protect fast-spiking interneurons against oxidative stress. *Proceedings of the National Academy of Sciences*.

Carulli, D., Rhodes, K. E., Brown, D. J., Bonnert, T. P., Pollack, S. J., Oliver, K., Strata, P. and Fawcett, J. W. (2006). Composition of perineuronal nets in the adult rat cerebellum and the cellular origin of their components. *Journal of Comparative Neurology* 494, 559-577.

Carulli, D., Pizzorusso, T., Kwok, J. C. F., Putignano, E., Poli, A., Forostyak, S., Andrews, M. R., Deepa, S. S., Glant, T. T. and Fawcett, J. W. (2010). Animals lacking link protein have attenuated perineuronal nets and persistent plasticity. *Brain* 133, 2331-2347.

Chang, E. F. and Merzenich, M. M. (2003). Environmental Noise Retards Auditory Cortical Development. *Science* 300, 498-502.

Chattopadhyaya, B., Di Cristo, G., Higashiyama, H., Knott, G. W., Kuhlman, S. J., Welker, E. and Huang, Z. J. (2004). Experience and Activity-Dependent Maturation of Perisomatic GABAergic Innervation in Primary Visual Cortex during a Postnatal Critical Period. *The Journal of Neuroscience* 24, 9598-9611.

Coles, C. H., Shen, Y., Tenney, A. P., Siebold, C., Sutton, G. C., Lu, W., Gallagher, J. T., Jones, E. Y., Flanagan, J. G. and Aricescu, A. R. (2011). Proteoglycan-Specific Molecular Switch for RPTPσ Clustering and Neuronal Extension. *Science* 332, 484-488.

Cristo, G. D., Wu, C., Chattopadhyaya, B., Ango, F., Knott, G., Welker, E., Svoboda, K. and Huang, Z. J. (2004). Subcellular domain-restricted GABAergic innervation in primary visual cortex in the absence of sensory and thalamic inputs. *Nature Neuroscience* 7, 1184-1186.

Csicsvari, J., Hirase, H., Czurkó, A., Mamiya, A. and Buzsáki, G. (1999). Oscillatory Coupling of Hippocampal Pyramidal Cells and Interneurons in the Behaving Rat. *The Journal of Neuroscience* 19, 274-287.

de Villers-Sidani, E., Chang, E. F., Bao, S. and Merzenich, M. M. (2007). Critical Period Window for Spectral Tuning Defined in the Primary Auditory Cortex (A1) in the Rat. *The Journal of Neuroscience* 27, 180-189.

Deepa, S. S., Carulli, D., Galtrey, C., Rhodes, K., Fukuda, J., Mikami, T., Sugahara, K. and Fawcett, J. W. (2006). Composition of Perineuronal Net Extracellular Matrix in Rat Brain: A different disaccharide composition for the net-associated proteoglycans. *Journal of Biological Chemistry* 281, 17789-17800.

Del Rio, J. A., De Lecea, L., Ferrer, I. and Soriano, E. (1994). The development of parvalbumin-immunoreactivity in the neocortex of the mouse. *Developmental Brain Research* 81, 247-259.

Des Rosiers, M., Sakurada, O., Jehle, J., Shinohara, M., Kennedy, C. and Sokoloff, L. (1978). Functional plasticity in the immature striate cortex of the monkey shown by the [14C]deoxyglucose method. *Science* 200, 447-449.

Dityatev, A., Bruckner, G., Dityateva, G., Grosche, J., Kleene, R. and Schachner, M. (2007). Activity-dependent formation and functions of chondroitin sulfate-rich extracellular matrix of perineuronal nets. *Dev Neurobiol* 67, 570-588.

Drager, U. C. (1978). Observations on monocular deprivation in mice. *Journal of Neurophysiology* 41, 28-42.

Erisir, A., Lau, D., Rudy, B. and Leonard, C. S. (1999). Function of Specific K+ Channels in Sustained High-Frequency Firing of Fast-Spiking Neocortical Interneurons. *Journal of Neurophysiology* 82, 2476-2489.

Ethell, I. M. and Ethell, D. W. (2007). Matrix metalloproteinases in brain development and remodeling: synaptic functions and targets. *J Neurosci Res* 85, 2813-2823.

Eysel, U. T. and Schweigart, G. (1999). Increased Receptive Field Size in the Surround of Chronic Lesions in the Adult Cat Visual Cortex. *Cerebral Cortex* 9, 101-109.

Fagiolini, M. and Hensch, T. K. (2000). Inhibitory threshold for critical-period activation in primary visual cortex. *Nature* 404, 183-186.

Fagiolini, M., Pizzorusso, T., Berardi, N., Domenici, L. and Maffei, L. (1994). Functional postnatal development of the rat primary visual cortex and the role of visual experience: Dark rearing and monocular deprivation. *Vision Research* 34, 709-720.

Fagiolini, M., Fritschy, J.-M., Löw, K., Möhler, H., Rudolph, U. and Hensch, T. K. (2004). Specific GABAA Circuits for Visual Cortical Plasticity. *Science* 303, 1681-1683.

Ferguson, J. E., Boldt, C. and Redish, A. D. (2009). Creating low-impedance tetrodes by electroplating with additives. *Sensors and Actuators A: Physical* 156, 388-393.

Franks, N. P. (2008). General anaesthesia: from molecular targets to neuronal pathways of sleep and arousal. *Nature Reviews Neuroscience* 9, 370-386.

Frenkel, M. Y. and Bear, M. F. (2004). How monocular deprivation shifts ocular dominance in visual cortex of young mice. *Neuron* 44, 917-924.

Freund, T. F. (2003). Interneuron diversity series: Rhythm and mood in perisomatic inhibition. *Trends in Neurosciences* 26, 489-495.

Galarreta, M. and Hestrin, S. (2002). Electrical and chemical synapses among parvalbumin fast-spiking GABAergic interneurons in adult mouse neocortex. *Proceedings of the National Academy of Sciences of the United States of America* 99, 12438-12443.

George Paxinos, C. W. (2007). The rat brain in stereotaxic coordinates. 6.

Girman, S. V., Sauve, Y. and Lund, R. D. (1999). Receptive field properties of single neurons in rat primary visual cortex. *J Neurophysiol* 82, 301-311.

Gogolla, N., Caroni, P., Luthi, A. and Herry, C. (2009). Perineuronal nets protect fear memories from erasure. *Science* 325, 1258-1261.

Golgi, C. (1898). Intorno alla struttura delle cellule nevose. *Bolet. Soc. Med.-Chir. Pavia* 1.

Gordon, J. A. and Stryker, M. P. (1996). Experience-Dependent Plasticity of Binocular Responses in the Primary Visual Cortex of the Mouse. *The Journal of Neuroscience* 16, 3274-3286.

Goritz, C., Dias, D. O., Tomilin, N., Barbacid, M., Shupliakov, O. and Frisen, J. (2011). A Pericyte Origin of Spinal Cord Scar Tissue. *Science* 333, 238-242.

Greenberg, D. S., Houweling, A. R. and Kerr, J. N. D. (2008). Population imaging of ongoing neuronal activity in the visual cortex of awake rats. *Nat Neurosci* 11, 749-751.

Greenough, W. T., Volkmar, F. R. and Juraska, J. M. (1973). Effects of rearing complexity on dendritic branching in frontolateral and temporal cortex of the rat. *Experimental Neurology* 41, 371-378.

Gundelfinger, E. D., Frischknecht, R., Choquet, D. and Heine, M. (2010). Converting juvenile into adult plasticity: a role for the brain's extracellular matrix. *European Journal of Neuroscience* 31, 2156-2165.

Hanover, J. L., Huang, Z. J., Tonegawa, S. and Stryker, M. P. (1999). Brain-derived neurotrophic factor overexpression induces precocious critical period in mouse visual cortex. *The Journal of neuroscience* 19.

Harauzov, A., Spolidoro, M., DiCristo, G., De Pasquale, R., Cancedda, L., Pizzorusso, T., Viegi, A., Berardi, N. and Maffei, L. (2010). Reducing intracortical inhibition in the adult visual cortex promotes ocular dominance plasticity. *The Journal of Neuroscience* 30, 361-371.

Hartig, W., Brauer, K., Bigl, V. and Bruckner, G. (1994). Chondroitin sulfate proteoglycan-immunoreactivity of lectin-labeled perineuronal nets around parvalbumin-containng neurons. *Brain Research* 635, 307-311.

Hatten, M. E., Liem, R. K. H., Shelanski, M. L. and Mason, C. A. (1991). Astroglia in CNS injury. *GLIA* 4, 233-243.

Headon, M. P. and Powell, T. P. (1973). Cellular changes in the lateral geniculate nucleus of infant monkeys after suture of the eyelids. *J Anat* 116, 135-145.

Hensch, T. K., Fagiolini, M., Mataga, N., Stryker, M. P., Baekkeskov, S. and Kash, S. F. (1998). Local GABA Circuit Control of Experience-Dependent Plasticity in Developing Visual Cortex. *Science* 282, 1504-1508.

Hill, J. J., Jin, K., Mao, X. O., Xie, L. and Greenberg, D. A. (2012). Intracerebral chondroitinase ABC and heparan sulfate proteoglycan glypican improve outcome from chronic stroke in rats. *Procedings of the National Acaddemy of Science U S A* 109, 9155-9160.

Hockfield, S. and McKay, R. D. (1983). A surface antigen expressed by a subset of neurons in the vertebrate central nervous system. *Proceedings of the National Academy of Science U S A* 80, 5758-5761.

Hockfield, S., Kalb, R. G., Zaremba, S. and Fryer, H. (1990). Expression of neural proteoglycans correlates with the acquisition of mature neuronal properties in the mammalian brain. *Cold Spring Harbor Symposia on Quantitative Biology* 55, 505-514.

Hofer, S. B., Mrsic-Flogel, T. D., Bonhoeffer, T. and Hubener, M. (2009). Experience leaves a lasting structural trace in cortical circuits. *Nature* 457, 313-317.

Horton, J. and Hocking, D. (1996). An adult-like pattern of ocular dominance columns in striate cortex of newborn monkeys prior to visual experience. *The Journal of Neuroscience* 16, 1791-1807.

Horton, J. C. and Hocking, D. R. (1996). Anatomical Demonstration of Ocular Dominance Columns in Striate Cortex of the Squirrel Monkey. *The Journal of Neuroscience* 16, 5510-5522.

Hrabetova, S., Masri, D., Tao, L., Xiao, F. R. and Nicholson, C. (2009). Calcium diffusion enhanced after cleavage of negatively charged components of brain extracellular matrix by chondroitinase ABC. *Journal of Physiology-London* 587, 4029-4049.

Huang, Z. J., Kirkwood, A., Pizzorusso, T., Porciatti, V., Morales, B., Bear, M. F., Maffei, L. and Tonegawa, S. (1999). BDNF regulates the maturation of inhibition and the critical period of plasticity in mouse visual cortex. *Cell* 98, 739-755.

Hubel, D. H. and Wiesel, T. N. (1959). Receptive fields of single neurones in the cat's striate cortex. *The Journal of physiology* 148, 574-591.

Hubel, D. H. and Wiesel, T. N. (1962). Receptive fields, binocular interaction and functional architecture in the cat's visual cortex. *The Journal of physiology* 160, 106-154.

Hubel, D. H., Wiesel, T. N. and LeVay, S. (1976). Functional Architecture of Area 17 in Normal and Monocularly Deprived Macaque Monkeys. *Cold Spring Harbor Symposia on Quantitative Biology* 40, 581-589.

Härtig, W., Derouiche, A., Welt, K., Brauer, K., Grosche, J., Mäder, M., Reichenbach, A. and Brückner, G. (1999). Cortical neurons immunoreactive for the potassium channel Kv3.1b subunit are predominantly surrounded by perineuronal nets presumed as a buffering system for cations. *Brain Research* 842, 15-29.

Iriki, A., Pavlides, C., Keller, A. and Asanuma, H. (1989). Long-term potentiation in the motor cortex. *Science* 245, 1385-1387.

Iwai, Y., Fagiolini, M., Obata, K. and Hensch, T. K. (2003). Rapid critical period induction by tonic inhibition in visual cortex. *Journal of Neuroscience* 23, 6695-6702.

Jenkins, W. M. and Merzenich, M. M. (1987). Reorganization of neocortical representations after brain injury: a neurophysiological model of the bases of recovery from stroke. *Progressive Brain Research* 71, 249-266.

Ji, D. and Wilson, M. A. (2006). Coordinated memory replay in the visual cortex and hippocampus during sleep. *Nature Neuroscience* 10, 100-107.

Johnson, J. S. and Newport, E. L. (1989). Critical period effects in second language learning: The influence of maturational state on the acquisition of English as a second language. *Cognitive Psychology* 21, 60-99.

Kádár, A., Wittmann, G., Liposits, Z. and Fekete, C. (2009). Improved method for combination of immunocytochemistry and Nissl staining. *Journal of neuroscience methods* 184, 115-118.

Kawaguchi, Y. and Kubota, Y. (1997). GABAergic cell subtypes and their synaptic connections in rat frontal cortex. *Cerebral Cortex* 7, 476-486.

Klausberger, T., Roberts, J. D. B. and Somogyi, P. (2002). Cell Type- and Input-Specific Differences in the Number and Subtypes of Synaptic GABAA Receptors in the Hippocampus. *The Journal of Neuroscience* 22, 2513-2521.

Kuffler, S. W. (1953). Discharge patterns and functional organization of mammalian retina. *Journal of Neurophysiology* 16, 37-68.

Kwok, J. C., Dick, G., Wang, D. and Fawcett, J. W. (2011). Extracellular matrix and perineuronal nets in CNS repair. *Developmental Neurobiology* 71, 1073-1089.
Lemaire, V., Tronel, S., Montaron, M.-F., Fabre, A., Dugast, E. and Abrous, D. N. (2012). Long-Lasting Plasticity of Hippocampal Adult-Born Neurons. *The Journal of Neuroscience* 32, 3101-3108.
Levy, W. B. and Steward, O. (1979). Synapses as associative memory elements in the hippocampal formation. *Brain Research* 175, 233-245.
Lewis, D. A., Hashimoto, T. and Volk, D. W. (2005). Cortical inhibitory neurons and schizophrenia. *Nature Reviews Neuroscience* 6, 312-324.
Lin, R., Rosahl, T. W., Whiting, P. J., Fawcett, J. W. and Kwok, J. C. F. (2011). 6-Sulphated Chondroitins Have a Positive Influence on Axonal Regeneration. *Plos One* 6.
Lundell, A., Olin, A. I., Morgelin, M., al-Karadaghi, S., Aspberg, A. and Logan, D. T. (2004). Structural basis for interactions between tenascins and lectican C-type lectin domains: Evidence for a crosslinking role for tenascins. *Structure* 12, 1495-1506.
Margolis, R. K., Margolis, R. U., Preti, C. and Lai, D. (1975). Distribution and metabolism of glycoproteins and glycosaminoglycans in subcellular fractions of brain. *Biochemistry* 14, 4797-4804.
Massey, J. M., Hubscher, C. H., Wagoner, M. R., Decker, J. A., Amps, J., Silver, J. and Onifer, S. M. (2006). Chondroitinase ABC Digestion of the Perineuronal Net Promotes Functional Collateral Sprouting in the Cuneate Nucleus after Cervical Spinal Cord Injury. *The Journal of Neuroscience* 26, 4406-4414.
Mataga, N., Nagai, N. and Hensch, T. K. (2002). Permissive proteolytic activity for visual cortical plasticity. *Proceedings of the National Academy of Sciences* 99, 7717-7721.
McKeon, R. J., Hoke, A. and Silver, J. (1995). Injury-induced proteoglycans inhibit the potential for laminin-mediated axon growth on astrocytic scars. *Experimental Neurology* 136, 32-43.
McKeon, R. J., Schreiber, R. C., Rudge, J. S. and Silver, J. (1991). Reduction of neurite outgrowth in a model of glial scarring following CNS injury is correlated with the expression of inhibitory molecules on reactive astrocytes. *Journal of Neuroscience* 11, 3398-3411.
McRae, P. A. and Porter, B. E. (2012). The perineuronal net component of the extracellular matrix in plasticity and epilepsy. *Neurochemistry Int* 61, 963-972.
McRae, P. A., Rocco, M. M., Kelly, G., Brumberg, J. C. and Matthews, R. T. (2007). Sensory deprivation alters aggrecan and perineuronal net expression in the mouse barrel cortex. *Journal of Neuroscience* 27, 5405-5413.
Mehta, M. R. and Wilson, M. A. (2000). From hippocampus to V1: Effect of LTP on spatio-temporal dynamics of receptive fields. *Neurocomputing* 32, 905-911.
Merzenich, M. M., Nelson, R. J., Stryker, M. P., Cynader, M. S., Schoppmann, A. and Zook, J. M. (1984). Somatosensory cortical map changes following digit amputation in adult monkeys. *The Journal of Comparative Neurology* 224, 591 -605.

Meyer, A. H., Katona, I., Blatow, M., Rozov, A. and Monyer, H. (2002). In Vivo Labeling of Parvalbumin-Positive Interneurons and Analysis of Electrical Coupling in Identified Neurons. *The Journal of Neuroscience* 22, 7055-7064.

Morawski, M., Bruckner, G., Jager, C., Seeger, G., Matthews, R. T. and Arendt, T. (2012). Involvement of perineuronal and perisynaptic extracellular matrix in Alzheimer's disease neuropathology. *Brain Pathology* 22, 547-561.

Morris, N. P. and Henderson, Z. (2000). Perineuronal nets ensheath fast spiking, parvalbumin-immunoreactive neurons in the medial septum/diagonal band complex. *European Journal of Neuroscience* 12, 828-838.

Mountcastle, V., Berman, A. and Davies, P. (1955). Topographic organization and modality representation in first somatic area of cat's cerebral cortex by method of single unit analysis. *American Journal of Physiology* 183, 464.

Mower, G. D. (1991). The effect of dark rearing on the time course of the postnatal critical period in cat visual cortex. *Developmental Brain Research* 58, 151-158.

Myers, J. P., Santiago-Medina, M. and Gomez, T. M. (2011). Regulation of axonal outgrowth and pathfinding by integrin-ECM interactions. *Developmental Neurobiology* 71, 901-923.

Niell, C. M. and Stryker, M. P. (2008). Highly Selective Receptive Fields in Mouse Visual Cortex. *The Journal of Neuroscience* 28, 7520-7536.

Niell, C. M. and Stryker, M. P. (2010). Modulation of visual responses by behavioral state in mouse visual cortex. *Neuron* 65, 472-479.

Nordby, J. C., Campbell, S. E. and Beecher, M. D. (2001). Late song learning in song sparrows. *Animal Behaviour* 61, 835-846.

Nusser, Z., Sieghart, W., Benke, D., Fritschy, J. M. and Somogyi, P. (1996). Differential synaptic localization of two major gamma-aminobutyric acid type A receptor alpha subunits on hippocampal pyramidal cells. *Proceedings of the National Academy of Sciences* 93, 11939-11944.

Oesterle, S. i. C. A. (2011). The Pipette Cookbook. Rev. G.

Pantazopoulos H, W. T. W. L. M. P. L. N. B. S. (2010). EXtracellular matrix-glial abnormalities in the amygdala and entorhinal cortex of subjects diagnosed with schizophrenia. *Archives of General Psychiatry* 67, 155-166.

Patz, S., Grabert, J., Gorba, T., Wirth, M. J. and Wahle, P. (2004). Parvalbumin Expression in Visual Cortical Interneurons Depends on Neuronal Activity and TrkB Ligands during an Early Period of Postnatal Development. *Cerebral Cortex* 14, 342-351.

Pindzola, R. R., Doller, C. and Silver, J. (1993). Putative inhibitory extracellular matrix molecules at the dorsal root entry zone of the spinal cord during development and after root and sciatic nerve lesions. *Developmental Biology* 156, 34-48.

Pizzorusso, T., Medini, P., Berardi, N., Chierzi, S., Fawcett, J. W. and Maffei, L. (2002). Reactivation of Ocular Dominance Plasticity in the Adult Visual Cortex. *Science* 298, 1248-1251.

Pizzorusso, T., Medini, P., Landi, S., Baldini, S., Berardi, N. and Maffei, L. (2006). Structural and functional recovery from early monocular deprivation in adult rats. *Proceedings of the National Academy of Sciences* 103, 8517-8522.

Prydz, K. and Dalen, K. T. (2000). Synthesis and sorting of proteoglycans. *J Cell Sci* 113 Pt 2, 193-205.

Pyka, M., Wetzel, C., Aguado, A., Geissler, M., Hatt, H. and Faissner, A. (2011). Chondroitin sulfate proteoglycans regulate astrocyte-dependent synaptogenesis and modulate synaptic activity in primary embryonic hippocampal neurons. *European Journal of Neuroscience* 33, 2187-2202.

Racine, R. J., Chapman, C. A., Trepel, C., Teskey, G. C. and Milgram, N. W. (1995). Post-activation potentiation in the neocortex. 4 multiple sessions required for induction of long-term potentiation in the chronic preparation. *Brain Research* 702, 87-93.

Rauch, U., Gao, P., Janetzko, A., Flaccus, A., Hilgenberg, L., Tekotte, H., Margolis, R. K. and Margolis, R. U. (1991). Isolation and characterization of developmentally regulated chondroitin sulfate and chondroitin/keratin sulfate proteoglycans of brain identified with monoclonal antibodies. *Journal of Biological Chemistry* 266, 14785-14801.

Rosenzweig, M. R., Bennett, E. L. and Krech, D. (1964). Cerebral effects of environmental complexity and training among adult rats. *Journal of Comparative and Physiological Psychology* 57, 438-439.

Rudy, B. and McBain, C. J. (2001). Kv3 channels: voltage-gated K+ channels designed for high-frequency repetitive firing. *Trends in Neurosciences* 24, 517-526.

Sato, M. and Stryker, M. P. (2008). Distinctive Features of Adult Ocular Dominance Plasticity. *The Journal of Neuroscience* 28, 10278-10286.

Schmalfeldt, M., Dours-Zimmermann, M. T., Winterhalter, K. H. and Zimmermann, D. R. (1998). Versican V2 is a major extracellular matrix component of the mature bovine brain. *Journal of Biological Chemistry* 273, 15758-15764.

Schwaller, B., Tetko, I. V., Tandon, P., Silveira, D. C., Vreugdenhil, M., Henzi, T., Potier, M. C., Celio, M. R. and Villa, A. E. (2004). Parvalbumin deficiency affects network properties resulting in increased susceptibility to epileptic seizures. *Mol Cell Neurosci* 25, 650-663.

Sekirnjak, C., Martone, M. E., Weiser, M., Deerinck, T., Bueno, E., Rudy, B. and Ellisman, M. (1997). Subcellular localization of the K+ channel subunit Kv3.1b in selected rat CNS neurons. *Brain Res* 766, 173-187.

Shatz, C. J. and Stryker, M. P. (1978). Ocular dominance in layer IV of cats visual-cortex and effects of monocular deprivation. *Journal of Physiology-London* 281, 267-&.

Snow, D. M., Atkinson, P. B., Hassinger, T. D., Letourneau, P. C. and Kater, S. B. (1994). Chondroitin sulfate proteoglycan elevates cytoplasmic calcium in DRG neurons. *Developmental Biology* 166, 87-100.

Soleman, S., Yip, P. K., Duricki, D. A. and Moon, L. D. (2012). Delayed treatment with chondroitinase ABC promotes sensorimotor recovery and plasticity after stroke in aged rats. *Brain* 135, 1210-1223.

Spolidoro, M., Putignano, E., Munafò, C., Maffei, L. and Pizzorusso, T. (2011). Inhibition of Matrix Metalloproteinases Prevents the Potentiation of Nondeprived-Eye Responses after Monocular Deprivation in Juvenile Rats. *Cerebral Cortex*.

Steriade, M., McCormick, D. A. and Sejnowski, T. J. (1993). Thalamocortical oscillations in the sleeping and aroused brain. *Science* 262, 679-685.

Sugiyama, S., Di Nardo, A. A., Aizawa, S., Matsuo, I., Volovitch, M., Prochiantz, A. and Hensch, T. K. (2008). Experience-Dependent Transfer of Otx2 Homeoprotein into the Visual Cortex Activates Postnatal Plasticity. *Cell* 134, 508-520.

Suttkus, A., Rohn, S., Jager, C., Arendt, T. and Morawski, M. (2012). Neuroprotection against iron-induced cell death by perineuronal nets - an in vivo analysis of oxidative stress. *Am J Neurodegener Dis* 1, 122-129.

Szuts, T. A., Fadeyev, V., Kachiguine, S., Sher, A., Grivich, M. V., Agrochao, M., Hottowy, P., Dabrowski, W., Lubenov, E. V., Siapas, A. G. et al. (2011). A wireless multi-channel neural amplifier for freely moving animals. *Nat Neurosci* 14, 263-269.

Tamás, G., Buhl, E. H. and Somogyi, P. (1997). Fast IPSPs elicited via multiple synaptic release sites by different types of GABAergic neurone in the cat visual cortex. *Journal of Physiology* 500, 715-738.

Thrane, A. S., Rangroo Thrane, V., Zeppenfeld, D., Lou, N., Xu, Q., Nagelhus, E. A. and Nedergaard, M. (2012). General anesthesia selectively disrupts astrocyte calcium signaling in the awake mouse cortex. *Proc Natl Acad Sci U S A* 109, 18974-18979.

Trepel, C. and Racine, R. J. (1998). Long-term potentiation in the neocortex of the adult, freely moving rat. *Cerebral Cortex* 8, 719-729.

Vaegan and Taylor, D. (1979). Critical period for deprivation amblyopia in children. *Transactions of the Ophthalmological Societies of the United Kingdom* 99, 432-439.

Van Hove, I., Lemmens, K., Van de Velde, S., Verslegers, M. and Moons, L. (2012). Matrix metalloproteinase-3 in the central nervous system: a look on the bright side. *J Neurochem* 123, 203-216.

Wang, B. S., Sarnaik, R. and Cang, J. (2010). Critical period plasticity matches binocular orientation preference in the visual cortex. *Neuron* 65, 246-256.

Wang, D. and Fawcett, J. (2012). The perineuronal net and the control of CNS plasticity. *Cell Tissue Res* 349, 147-160.

Weiser, M., Bueno, E., Sekirnjak, C., Martone, M. E., Baker, H., Hillman, D., Chen, S., Thornhill, W., Ellisman, M. and Rudy, B. (1995). The potassium channel subunit KV3.1b is localized to somatic and axonal membranes of specific populations of CNS neurons. *J Neurosci* 15, 4298-4314.

Whishaw, I. and Vanderwolf, C. (1973). Hippocampal EEG and behavior: change in amplitude and frequency of RSA (theta rhythm) associated with spontaneous and learned movement patterns in rats and cats. *Behavioral biology* 8, 461-484.

Wiesel, T. N. and Hubel, D. H. (1963). Single-cell responses in striate cortex of kittens deprived of vision. *Journal of Neurophysiology* 26, 1003-1017.

Wilson, F. A., O'Scalaidhe, S. P. and Goldman-Rakic, P. S. (1994). Functional synergism between putative gamma-aminobutyrate-containing neurons and pyramidal neurons in prefrontal cortex. *Proceedings of the National Academy of Science U S A* 91, 4009- 4013.

Yamada, H., Fredette, B., Shitara, K., Hagihara, K., Miura, R., Ranscht, B., Stallcup, W. B. and Yamaguchi, Y. (1997). The brain chondroitin sulfate proteoglycan brevican associates with astrocytes ensheathing cerebellar glomeruli and inhibits neurite outgrowth from granule neurons. *Journal of Neuroscience* 17, 7784-7795.

Yamaguchi, Y. (2000). Lecticans: organizers of the brain extracellular matrix. *Cellular and Molecular Life Sciences* 57, 276-289.

Ye, Q. and Miao, Q. L. (2013). Experience-dependent development of perineuronal nets and chondroitin sulfate proteoglycan receptors in mouse visual cortex. *Matrix Biol*ogy

Ylinen, A., Soltesz, I., Bragin, A., Penttonen, M., Sik, A. and Buzsaki, G. (1995). Intracellular correlates of the hippocampal theta-rhythm in identified pyramidal cells, granule cells, and basket cells. *Hippocampus* 5, 78-90.

Zafra, F., Hengerer, B., Leibrock, J., Thoenen, H. and Lindholm, D. (1990). Activity dependent regulation of BDNF and NGF mRNAs in the rat hippocampus is mediated by non-NMDA glutamate receptors. *EMBO Journal* 9, 3545-3550.

5 Appendix

5.1 List of abbreviations

AP	anterioposterior
aCSF	artificial cerebrospinal fluid
BDNF	Brain-derived neurotrophic factor
chABC	Chondroitinase ABC
CNS	central nervous system
CP	critical period
CS	chondroitin sulfate
CSPG	chondroitin sulfate proteoglycan
DAB	diaminobenzidine
dLGN	dorsal lateral geniculate nucleus
DV	dorsoventral
ECM	extracellular matrix
EEG	electroencephalogram
GABA	gamma-amino butyric acid
GFAP	glial fibrillary acidic protein
HSPG	heparan sulfate proteoglycan
KSPG	keratan sulfate proteoglycan
LTD	long-term depression

LTP	long-term potentiation
MMP	matrix metalloproteinase
tPA	tissue activated plasminogen
MD	monocular deprivation
ML	mediolateral
OD	ocular dominance
ODI	ocular dominance index
OSI	orientation selectivity index
Otx2	Orthodenticle homeobox protein 2
PBS	phosphate-buffered saline
PFA	paraformaldehyde
PG	proteoglycan
PNN	perineuronal net
PV	parvalbumin
s.c.	subcutaneous
SEM	standard error of the mean
V1	primary visual cortex
VEP	visually evoked potentials
WFA	*Wisteria floribunda* agglutinin

5.2 Solutions used for immunohistochemistry and histochemistry

5.2.1 10X PBS

80g of NaCl

2.0g of KCl

14.4g of Na_2HPO_4

2.4g of KH_2PO_4

Dissolve in 800 ml dH_2O, adjust pH to 7.4, and adjust volume to 1L

Dilute 1:10 with dH_2O for 1X solution

5.2.2 TS-PBS

3% Normal Goat Serum

0.3% Triton X-100

Dissolve in 1 X PBS

5.2.3 T-PBS

0.3% Triton X-100 in 1 X PBS

5.2.4 TNS

6g Trizma-HCl

1L dH_2O, adjust pH to 7.4 with 1M NaOH

5.2.5 Tris-HCl 0.05M

6.06 g Tris

1L dH_2O, adjust pH to 7.6

5.2.6 96% ethanol with acetic acid

500 mL absolute ethanol

2.5 mL acetic acid

5.2.7 Cresyl violet staining solution

0.5 g cresyl violet acetate

1.25 mL glacial acetic acid

500 mL dH_20

Heat to 60°C and filter before use

5.2.8 4% paraformaldehyde (PFA)

40 g PFA

1 L 1X PBS

Heat to 50-60°C, leave with stirring until everything is dissolved (3-4 hours)

Filter before use

5.3 Immunohistochemistry and histochemistry protocols

5.3.1 Staining for PNNs, light microscopy

Primary antibody**:** biotinylated *Wisteria florubinda* lectin (Sigma L-1516)
Secondary antibody**:** anti-rabbit IgG (also reactive against biotin) (ABC kit, Vector PK-6101)

1. Rinse sections with 1 X PBS, 3 x 5 minutes.

2. Block sections with TS-PBS for 1hour at room temperature.

3. Dilute WFA-biotin in TS-PBS 1:200, add WFA-biotin to sections. Keep in 4°C overnight.

4. Rinse sections with T-PBS, 3 x 5 minutes.

5. Quenching endogenous peroxidase: 1,5% H_2O_2 in ddH_2O. Incubate for 3 minutes, rinse with T-PBS for 5 min.

6. Incubate with 2° antibody for 1h at room temperature. (2° AB: 135 µL Normal Goat Serum, 45µL Reagent B, 10mL PBS).

7. Rinse with T-PBS, 3 x 10 minutes. During the wait, prepare the DAB pellet **under fume hood**: 15 mL Tris-HCl to 1 pellet (10 mg), heat to 50°C with magnetic stirrer (takes approx. 2 hours). Remains from this solution can be stored at 4 °C and activated later by adding H_2O_2.

8. ABC staining solution: 90 µL Reagent A, 10 mL PBS, 90 µL Reagent B. Incubate at room temperature 30 minutes.

9. Add ABC solution to sections, incubate min. 1 hour at room temperature. From this point, sections should be in separate wells – makes visualizing the progression of the DAB reaction easier.

10. Rinse sections with TNS, 3 x 15 minutes.

11. Add 12 µL H_2O_2 to DAB solution, filter it and add the DAB/H_2O_2 solution to sections under fume hood. Incubate until desired color is observed (5-10 min).

12. Stop the reaction with TNS, rinse minimum 3 times with TNS. Mount the sections on slides using a fine brush and TNS. Wipe off excess TNS and dry sections at 37 °C.

13. Dehydrate sections with 95% EtOH, then 100%EtOH and finally xylene. Secure sections with DRX/Entellan and a cover slip. Remove Entellan remains on cover slip by immersing in xylene for 1 minute.

5.3.2 Staining for glia cells

Primary antibody: rabbit anti-Glial fibrillary acidic protein (DakoCytomation Z0334)
Secondary antibody: anti rabbit IgG (ABC kit, Vector PK-6101)

1. Rinse sections with 1 X PBS, 3 x 5 minutes.

2. Block sections with TS-PBS for 1hour at room temperature.

3. Dilute GFAP in T-PBS 1:500, add GFAP to sections. Keep at 4°C overnight.

4. Rinse sections with T-PBS, 3 x 5 minutes.

5. Quenching endogenous peroxidase: 2% H_2O_2 in ddH_2O. Incubate for 3 minutes, rinse with T-PBS for 5 minutes.

6. Incubate with 2° antibody for 1h at room temperature. (2° AB: 135 µL Normal Goat Serum, 45µL Reagent B, 10mL PBS).

7. Rinse with T-PBS, 3 x 10 minutes. During the wait, prepare the DAB pellet **under fume hood**: 15 mL Tris-HCl to 1 pellet (10 mg), heat to 50°C with magnetic stirrer (takes approx. 2 hours). Remains from this solution can be stored at 4 °C and activated later by adding H_2O_2.

8. ABC staining solution: 90 µL Reagent A, 10 mL PBS, 90 µL Reagent B. Incubate at room temperature 30 minutes.

9. Add ABC solution to sections, incubate min. 1 hour at room temperature.

10. Rinse sections with TNS, 3 x 15 minutes.

11. Add 12 µL H_2O_2 to DAB solution, filter it and add the DAB/H_2O_2 solution to sections under fume hood. Incubate until desired color is observed (3-5 min).

12. Stop the reaction with TNS, rinse minimum 3 times with TNS. Mount the sections on slides using a fine brush and TNS. Wipe off excess TNS and dry sections at 37 °C.

13. Dehydrate sections with 95% EtOH, then 100%EtOH and finally xylene. Secure sections with DRX/Entellan and a cover slip. Remove Entellan remains on cover slip by immersing in xylene for 1 minute.

5.3.3 Staining for Nissl bodies with cresyl vioet

1. Immerse sections in a 1:1 chloroform: absolute ethanol solution overnight, in order to secure sections to glass

2. dH_2O for 2 minutes

3. Cresyl violet solution for 2-6 minutes

4. dH_2O 2 minutes

5. 70% ethanol 2 minutes

6. 80% ethanol 2 minutes

7. 90% ethanol 2 minutes

8. 96% ethanol with acetic acid 1-5 minutes, depending on how much color is lost

9. Absolute ethanol 2 minutes

10. Xylene 5-15 minutes

11. Mount sections with Entellan and a cover slip. Leave in fume hood overnight.

Alcohol solutions are made with absolute ethanol, diluted with dH_2O.

5.4 Tetrode tracks

Not all the brains from the animals used are shown below. This is due to the fact that three of them were ruined during sectioning or staining, and the remaining are yet to be sectioned.

A)

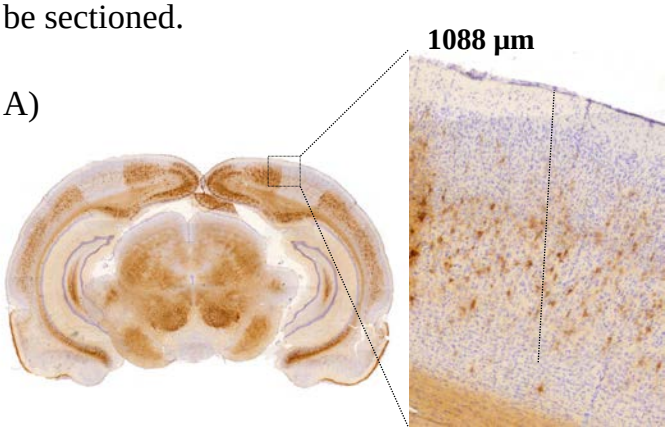

B)

C)

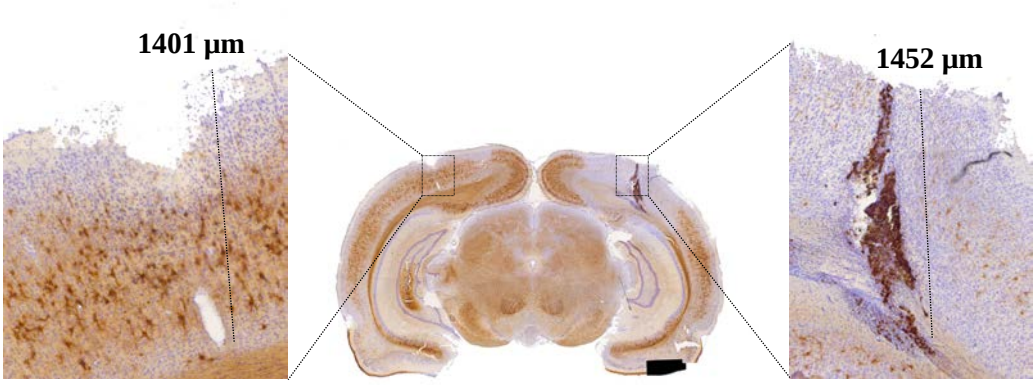

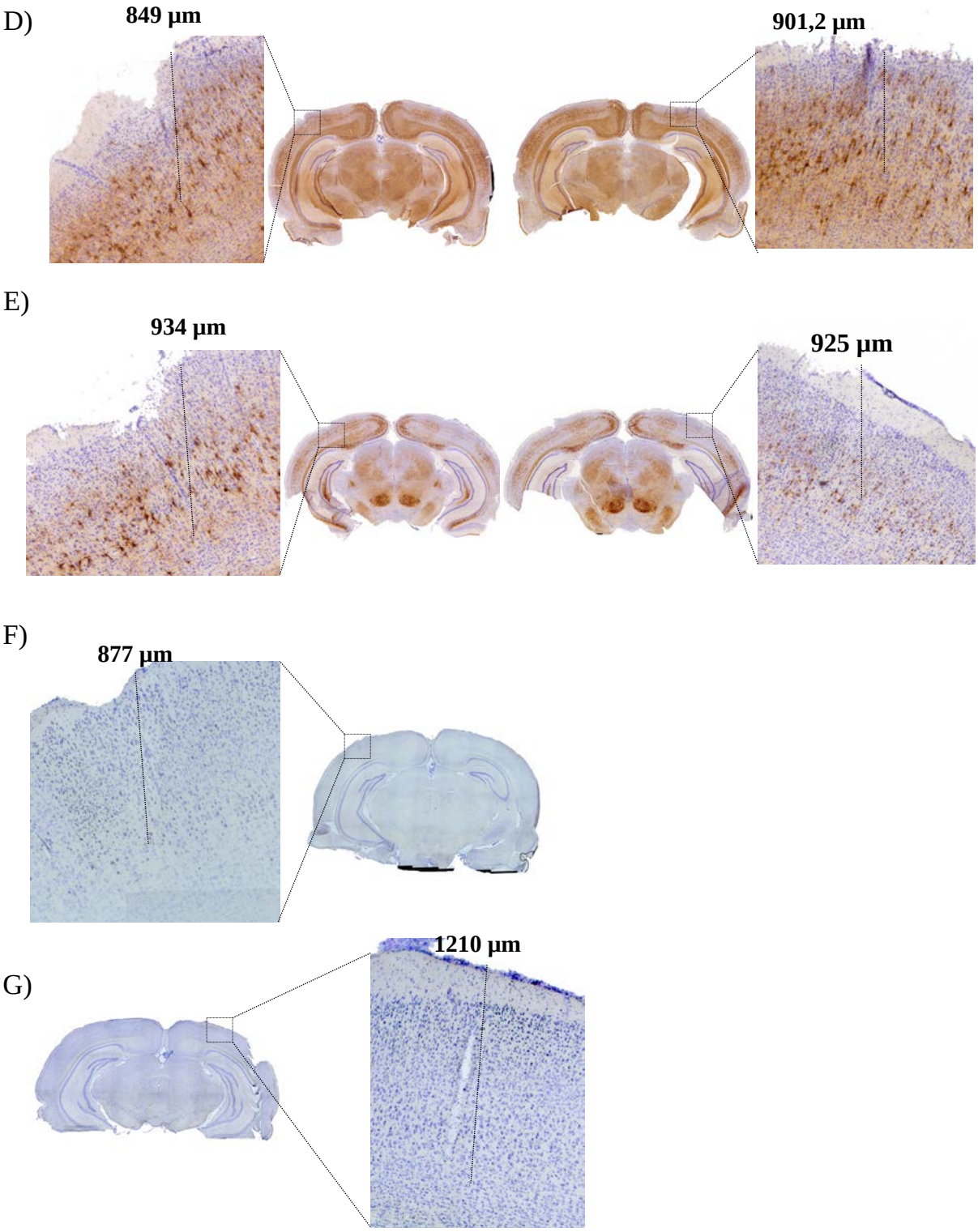

Figure 5.1: Tetrode tracks in V1 in chABC injected animals and control animals. The track can be seen just to the left of the dotted line. **A-F)** Sections are stained with *Wisteria floribunda* agglutinin to visualize perineuronal nets and for Nissl bodies to visualize the tetrode track. **F-G)** Sections from animals used as controls. The sections are stined for Nissl bodies to visualize the tetrdeo track.)